Isogeometric Kirchhoff–Love shell formulations for general hyperelastic materials

Josef Kiendl[a,*], Ming-Chen Hsu[b], Michael C. H. Wu[b], Alessandro Reali[a,c,d]

[a] *Dipartimento di Ingegneria Civile ed Architettura, Università degli Studi di Pavia, Via Ferrata 3, 27100 Pavia, Italy*
[b] *Department of Mechanical Engineering, Iowa State University, 2025 Black Engineering, Ames, IA 50011, USA*
[c] *Istituto di Matematica Applicata e Tecnologie Informatiche – CNR, Via Ferrata 1, 27100 Pavia, Italy*
[d] *Technische Universität München – Institute for Advanced Study, Lichtenbergstraße 2a, 85748 Garching, Germany*

Abstract

We present formulations for compressible and incompressible hyperelastic thin shells which can use general 3D constitutive models. The necessary plane stress condition is enforced analytically for incompressible materials and iteratively for compressible materials. The thickness stretch is statically condensed and the shell kinematics are completely described by the first and second fundamental forms of the midsurface. We use C^1-continuous isogeometric discretizations to build the numerical models. Numerical tests, including structural dynamics simulations of a bioprosthetic heart valve, show the good performance and applicability of the presented methods.

Keywords: Isogeometric; Kirchhoff–Love; Thin shell; Hyperelastic; Finite strain; Nonlinear material; Incompressibility

1. Introduction

Thin shells can undergo large displacements and rotations while exhibiting only small strains, especially for bending-dominated deformations, due to their geometric dimensions. Accordingly, a geometrically nonlinear approach is often employed, where nonlinear kinematics are accounted for but a linear strain-stress relation is assumed, corresponding to the St. Venant–Kirchhoff constitutive model. However, this approach is not appropriate in the presence of large membrane strains and when nonlinear elastic constitutive laws, typically used for the modeling of rubber-like materials and biological tissues, need to be employed. In such cases, a fully nonlinear formulation, including both kinematic and constitutive nonlinearities, needs to be adopted.

It is well known that thin shells can be modeled appropriately with the classical Kirchhoff–Love kinematics, but the necessary C^1 continuity inherent in such models has always been a major obstacle for the development of efficient finite element formulations. As a consequence, thick

*Corresponding author
Email address: josef.kiendl@unipv.it (Josef Kiendl)

The final publication is available at Elsevier via http://dx.doi.org/10.1016/j.cma.2015.03.010

shell formulations based on Reissner–Mindlin kinematics requiring only C^0 continuity are much more widespread in finite element shell analysis [1]. In the context of finite strains, higher order shell models including transverse normal strains [2–6] or solid-shells [7–9], just to name a few, are usually employed since they facilitate the implementation of general 3D material laws. As a matter of fact, the formulation of C^1 conforming thin shell finite elements is possible and has been presented, e.g., in [10, 11], including also finite strains. However, these elements are very complicated and computationally expensive (in the mentioned references, triangles with 54 degrees of freedom per element have been used) and, therefore, of little practical use. A possible way to use C^0 elements in thin shell formulations is to compute curvatures in an approximative way by the surface normals of surrounding elements, see [12, 13]. Alternative, smooth discretization techniques like meshless methods and subdivision surfaces allow a very natural implementation of thin shell models, see [14] for a meshless implementation and [15, 16] for the subdivision surfaces approach.

Isogeometric analysis (IGA) [17] is a new trend in computational mechanics, which can be considered as an extension of finite element analysis where functions typically used in Computer Aided Design (CAD) are adopted as basis functions for analysis. The most widespread functions in both CAD and IGA up to today are Non-Uniform Rational B-Splines (NURBS). An interesting alternative is T-splines [18, 19], which allow for local refinement and watertight modeling and have also been applied successfully in the context of IGA, see e.g. [20–23]. While the initial motivation of IGA was to better integrate design and analysis by this common geometry description, it has also been found in various studies that IGA has superior convergence properties compared to classical finite elements on a per degree-of-freedom basis [24–26]. Over the last years, IGA has attracted enormous interest in nearly all fields of computational mechanics and it also gave new life to the development of shell formulations, including rotation-free shells [27–29], Reissner–Mindlin shells [30–33], blended shells [34], hierarchic shells [35], and solid shells [36–40]. The high continuity naturally inherent in the isogeometric basis functions allows for a straightforward implementation of C^1 thin shell models. In [27], an isogeometric formulation for geometrically nonlinear Kirchhoff–Love shells has been firstly presented. The formulation is rotation-free and purely surface-based, which means that the shell kinematics are completely described by the mid-surface's metric and curvature properties. This also allows for a direct integration of IGA into CAD systems, which are ususally based on surface geometry models [41, 42]. The lack of rotational degrees of freedom also permits a direct coupling of structures and fluids in fluid–structure interaction (FSI) applications, see [22, 43, 44]. Furthermore, this shell model has been applied to wind turbine blade modeling [45, 46], isogeometric cloth modeling [47], explicit finite strain analysis of membranes [48], and for the modeling of fracture within an extended IGA approach [49].

In the present paper, we extend the isogeometric shell model presented in [27] to the large strain regime, including compressible and incompressible nonlinear hyperelastic materials. We develop the formulations such that arbitrary 3D constitutive laws can be used for the shell analysis. The transverse normal strain, which cannot be neglected in the case of large strains, is statically condensed using the plane stress condition (in this paper we adopt the commonly accepted, although incorrect, use of the term "plane stress" for referring to the state of zero transverse normal stress). As a consequence, the thickness stretch is not considered as additional variable and the shell kinematics are still completely described by the metric and curvature variables of the midsurface. The imposition of the plane stress condition is done differently for compressible and incompressible materials. While for the former it is obtained by an iterative update of the deformation tensor, it can be solved analytically for the latter by using the incompressibility constraint. In both approaches we derive the formulations considering a general 3D strain energy function, such that arbitrary 3D constitutive models, both compressible and incompressible, can be used for the shell formulation straight away. We present the derivation from the continuum to the shell model in detail using index notation in a convective curvilinear frame.

The paper is structured as follows: In Section 2, we introduce some notation convention used in this paper. Section 3 presents geometrical basics for the shell description while in Section 4, the shell kinematics are derived. In Section 5, the constitutive equations are presented with a focus on the consistent derivation from the 3D continuum to the shell model via the plane stress condition. In Section 6, we show the variational formulation, with detailed linearization of the strain variables to be found in Appendix C. In Section 7, we discuss the isogeometric discretization and implementation details. In Section 8, we present numerical tests including benchmark examples for which analytical solutions are available, as well as the application to biomechanics problems, namely structural dynamics simulations of a bioprosthetic aortic valve, which demonstrate the validity and applicability of the presented methods. Finally, conclusions are drawn in Section 9.

2. Notation

The following notation is used: italic letters a, A indicate scalars, lower case bold letters $\mathbf{a}$ indicate vectors, and upper case bold letters $\mathbf{A}$ indicate second order tensors. Geometric variables indicated by $(\mathring{\cdot})$ refer to the undeformed configuration. The following symbols for different vector products are used: $\mathbf{a} \cdot \mathbf{b}$ denotes the scalar product, $\mathbf{a} \times \mathbf{b}$ the cross product, and $\mathbf{a} \otimes \mathbf{b}$ the dyadic or tensor product. The determinant of a tensor is denoted by $\det(\mathbf{A})$, while the determinant of a matrix is denoted by $|A_{ij}|$. Compact notation is used only when convenient for the presentation of general equations, while the detailed derivations are written in index notation. Latin indices take on values $\{1, 2, 3\}$, while Greek indices take on values $\{1, 2\}$, and summation convention of repeated indices is used. Convective curvilinear coordinates θ^i are used, where θ^α are the surface coordinates of

the shell's midsurface and θ^3 is the thickness coordinate. Partial derivatives with respect to θ^i are indicated as $(\cdot)_{,i} = \partial(\cdot)/\partial\theta^i$.

3. Shell geometry

Due to the Kirchhoff hypothesis of straight and normal cross sections, the shell continuum can be described by the midsurface and the normal vector field. Given a point $\mathbf{r}$ on the midsurface, the tangent base vectors of the midsurface are obtained by $\mathbf{a}_\alpha = \mathbf{r}_{,\alpha}$. The metric coefficients of the midsurface are obtained by the first fundamental form:

$$a_{\alpha\beta} = \mathbf{a}_\alpha \cdot \mathbf{a}_\beta \ . \tag{1}$$

Curvature coefficients of the midsurface are obtained by the second fundamental form:

$$b_{\alpha\beta} = -\mathbf{a}_\alpha \cdot \mathbf{a}_{3,\beta} = -\mathbf{a}_\beta \cdot \mathbf{a}_{3,\alpha} = \mathbf{a}_{\alpha,\beta} \cdot \mathbf{a}_3 \ , \tag{2}$$

where $\mathbf{a}_3$ denotes the unit normal vector:

$$\mathbf{a}_3 = \frac{\mathbf{a}_1 \times \mathbf{a}_2}{|\mathbf{a}_1 \times \mathbf{a}_2|} \ . \tag{3}$$

A point $\mathbf{x}$ in the shell continuum can be described by a point on the midsurface $\mathbf{r}$ and a fiber director, which is identified as $\mathbf{a}_3$ due to the Kirchhoff hypothesis:

$$\mathbf{x} = \mathbf{r} + \theta^3 \, \mathbf{a}_3 \ , \tag{4}$$

with $-h/2 \leq \theta^3 \leq h/2$, h being the shell thickness. The base vectors at a point in the shell continuum are denoted by $\mathbf{g}_i = \mathbf{x}_{,i}$ and can be expressed by those of the midsurface $\mathbf{a}_i$ as follows:

$$\mathbf{g}_\alpha = \mathbf{a}_\alpha + \theta^3 \, \mathbf{a}_{3,\alpha} \ , \tag{5}$$

$$\mathbf{g}_3 = \mathbf{a}_3 \ . \tag{6}$$

The metric coefficients at a point in the shell continuum are then obtained as:

$$g_{\alpha\beta} = a_{\alpha\beta} - 2\theta^3 b_{\alpha\beta} + \left(\theta^3\right)^2 \mathbf{a}_{3,\alpha} \cdot \mathbf{a}_{3,\beta} \ , \tag{7}$$

$$g_{\alpha 3} = g_{3\alpha} = \mathbf{a}_\alpha \cdot \mathbf{a}_3 + \theta^3 \mathbf{a}_{3,\alpha} \cdot \mathbf{a}_3 = 0 \ , \tag{8}$$

$$g_{33} = a_{33} = 1 \ . \tag{9}$$

Corresponding to the classical assumption of a linear strain distribution through the thickness, the quadratic term in Eq. (7) is neglected:

$$g_{\alpha\beta} = a_{\alpha\beta} - 2\theta^3 b_{\alpha\beta} \, . \tag{10}$$

The metric coefficients can be gathered in matrix form as follows:

$$g_{ij} = \begin{pmatrix} g_{11} & g_{12} & 0 \\ g_{21} & g_{22} & 0 \\ 0 & 0 & 1 \end{pmatrix} . \tag{11}$$

The contravariant metric coefficients are obtained by the inverse matrix of the covariant coefficients, $[g^{ij}] = [g_{ij}]^{-1}$. According to Eq. (11), we obtain:

$$g^{ij} = \begin{pmatrix} g^{11} & g^{12} & 0 \\ g^{21} & g^{22} & 0 \\ 0 & 0 & 1 \end{pmatrix} \qquad \text{with} \quad [g^{\alpha\beta}] = [g_{\alpha\beta}]^{-1} \, . \tag{12}$$

The contravariant metric coefficients can be used to compute the contravariant base vectors $\mathbf{g}^i$, defined by the Kronecker delta property $\mathbf{g}^i \cdot \mathbf{g}_j = \delta^i_j$, as follows:

$$\mathbf{g}^\alpha = g^{\alpha\beta}\mathbf{g}_\beta \, , \tag{13}$$

$$\mathbf{g}^3 = \mathbf{g}_3 \, . \tag{14}$$

Eqs. (1)–(14) hold analogously for the undeformed configuration ($\mathring{a}_{\alpha\beta}$, $\mathring{b}_{\alpha\beta}$, etc.). Note that these equations do not reflect the thickness change in the deformed configuration, which is accounted for in the kinematic and constitutive equations presented in Sections 4 and 5.

For a tensor expressed in the contravariant basis of the undeformed configuration, $\mathbf{A} = A_{ij}\mathring{\mathbf{g}}^i \otimes \mathring{\mathbf{g}}^j$, as it is typically the case for the deformation and strain tensors in a Lagrangian description (see also Section 4), the trace and determinant are obtained as:

$$\mathrm{tr}(\mathbf{A}) = A_{ij}\,\mathring{g}^{ij} = A_{\alpha\beta}\,\mathring{g}^{\alpha\beta} + A_{33} \, , \tag{15}$$

$$\det(\mathbf{A}) = \frac{|A_{ij}|}{|\mathring{g}_{ij}|} = \frac{|A_{ij}|}{|\mathring{g}_{\alpha\beta}|} \, . \tag{16}$$

4. Kinematics

The displacement vector $\mathbf{u}$ describes the deformation of a point on the midsurface from the undeformed to the deformed configuration $\mathbf{r} = \mathring{\mathbf{r}} + \mathbf{u}$. For a point in the shell continuum we

can write $\mathbf{x} = \mathring{\mathbf{r}} + \mathbf{u} + \theta^3 \mathbf{a}_3(\mathring{\mathbf{r}} + \mathbf{u})$. We remark that in the following, kinematic variables are not expressed as functions of the displacements $\mathbf{u}$ but in terms of geometric quantities in the deformed and undeformed configurations. Strain and stress variables are expressed in terms of the right Cauchy-Green deformation tensor $\mathbf{C} = \mathbf{F}^T\mathbf{F}$, where $\mathbf{F}$ is the deformation gradient:

$$\mathbf{F} = \frac{\mathrm{d}\mathbf{x}}{\mathrm{d}\mathring{\mathbf{x}}} = \mathbf{g}_i \otimes \mathring{\mathbf{g}}^i \,, \tag{17}$$

$$\mathbf{C} = \mathbf{F}^T\mathbf{F} = \mathbf{g}_i \cdot \mathbf{g}_j \, \mathring{\mathbf{g}}^i \otimes \mathring{\mathbf{g}}^j = g_{ij} \, \mathring{\mathbf{g}}^i \otimes \mathring{\mathbf{g}}^j \,. \tag{18}$$

According to Eq. (18), which is valid for a general 3D continuum, the covariant coefficients of the deformation tensor are identical to the metric coefficients of the deformed configuration, i.e., $C_{ij} = g_{ij}$. In the shell model, this relation does not hold for the transverse normal direction, i.e., $C_{33} \neq g_{33}$, since $g_{33} \equiv 1$ due to the definition in Eq. (6), while C_{33} needs to describe the actual thickness deformation. Accordingly, we represent the deformation tensor $\mathbf{C} = C_{ij} \, \mathring{\mathbf{g}}^i \otimes \mathring{\mathbf{g}}^j$ by:

$$C_{ij} = \begin{pmatrix} g_{11} & g_{12} & 0 \\ g_{21} & g_{22} & 0 \\ 0 & 0 & C_{33} \end{pmatrix} . \tag{19}$$

As will be shown in Section 5, C_{33} can be computed from the in-plane components $g_{\alpha\beta}$ using the plane stress condition. The inverse of the deformation tensor, $\mathbf{C}^{-1} = \bar{C}^{ij} \, \mathring{\mathbf{g}}_i \otimes \mathring{\mathbf{g}}_j$, is obtained as:

$$\bar{C}^{ij} = \begin{pmatrix} g^{11} & g^{12} & 0 \\ g^{21} & g^{22} & 0 \\ 0 & 0 & C_{33}^{-1} \end{pmatrix} . \tag{20}$$

The trace of $\mathbf{C}$ is obtained according to Eq. (15):

$$\mathrm{tr}(\mathbf{C}) = g_{\alpha\beta} \, \mathring{g}^{\alpha\beta} + C_{33} \,, \tag{21}$$

and the determinant is obtained according to Eq. (16):

$$\det(\mathbf{C}) = \frac{|g_{\alpha\beta}| \, C_{33}}{|\mathring{g}_{\alpha\beta}|} = J_o^2 \, C_{33} \,, \tag{22}$$

where we defined the in-plane Jacobian determinant J_o as:

$$J_o = \sqrt{\frac{|g_{\alpha\beta}|}{|\mathring{g}_{\alpha\beta}|}} \,, \tag{23}$$

which is related to the Jacobian determinant $J = \det(\mathbf{F})$ by:

$$J = J_o \sqrt{C_{33}} \, . \tag{24}$$

The invariants of the deformation tensor, I_1, I_2, I_3, and their relation to the principal stretches $\lambda_1, \lambda_2, \lambda_3$, are given in the following equations:

$$I_1 = \mathrm{tr}(\mathbf{C}) = \lambda_1^2 + \lambda_2^2 + \lambda_3^2 \, , \tag{25}$$

$$I_2 = \frac{1}{2}\left(\mathrm{tr}(\mathbf{C})^2 - \mathrm{tr}(\mathbf{C}^2)\right) = \lambda_1^2\lambda_2^2 + \lambda_1^2\lambda_3^2 + \lambda_2^2\lambda_3^2 \, , \tag{26}$$

$$I_3 = \det(\mathbf{C}) = \lambda_1^2\lambda_2^2\lambda_3^2 \, . \tag{27}$$

In the shell model, λ_3 is the thickness stretch and $\lambda_3 = \sqrt{C_{33}}$.

As strain measure, we use the Green–Lagrange strain $\mathbf{E} = E_{ij}\, \mathring{\mathbf{g}}^i \otimes \mathring{\mathbf{g}}^j$, with:

$$E_{ij} = \frac{1}{2}(C_{ij} - \mathring{g}_{ij}) \, . \tag{28}$$

Transverse shear strains vanish, $E_{\alpha 3} = 0$, while the transverse normal strain, $E_{33} \neq 0$, is statically condensed as will be shown in Section 5. Accordingly, only in-plane strain components are considered for the shell kinematics:

$$E_{\alpha\beta} = \frac{1}{2}(g_{\alpha\beta} - \mathring{g}_{\alpha\beta}) \, . \tag{29}$$

Using Eq. (10), the strains can be expressed in terms of the metric and curvature coefficients of the midsurface:

$$E_{\alpha\beta} = \frac{1}{2}\left((a_{\alpha\beta} - \mathring{a}_{\alpha\beta}) - 2\theta^3(b_{\alpha\beta} - \mathring{b}_{\alpha\beta})\right) \, . \tag{30}$$

Introducing membrane strains $\varepsilon_{\alpha\beta}$ and curvature changes $\kappa_{\alpha\beta}$, obtained by the metric and curvature coefficients of the midsurface as:

$$\varepsilon_{\alpha\beta} = \frac{1}{2}(a_{\alpha\beta} - \mathring{a}_{\alpha\beta}) \, , \tag{31}$$

$$\kappa_{\alpha\beta} = \mathring{b}_{\alpha\beta} - b_{\alpha\beta} \, , \tag{32}$$

the strains in the shell continuum can be expressed as:

$$E_{\alpha\beta} = \varepsilon_{\alpha\beta} + \theta^3 \kappa_{\alpha\beta} \, , \tag{33}$$

where the first term is related to membrane deformation and the second one to bending. Accordingly, $\kappa_{\alpha\beta}$ is also called bending (pseudo-)strain.

5. Constitutive equations

An arbitrary isotropic hyperelastic constitutive model, described by a strain energy function $\psi(\mathbf{C})$, is considered. In the following, we present a consistent and general derivation from the 3D continuum to the shell model for both compressible and incompressible materials.

In the variational formulation we use the second Piola–Kirchhoff stress tensor, $\mathbf{S} = S^{ij}\,\mathring{\mathbf{g}}_i \otimes \mathring{\mathbf{g}}_j$, which is energetically conjugate to the Green–Lagrange strain tensor:

$$S^{ij} = \frac{\partial \psi}{\partial E_{ij}} = 2\frac{\partial \psi}{\partial C_{ij}} \,. \tag{34}$$

Since the second Piola–Kirchhoff stress tensor does not represent physical stresses, the Cauchy stress tensor, $\boldsymbol{\sigma} = J^{-1}\mathbf{F}\,\mathbf{S}\,\mathbf{F}^T$, also called "true stress", is used for stress recovery.

The total differential $\mathrm{d}S^{ij}$ is obtained by the following linearization:

$$\mathrm{d}S^{ij} = \frac{\partial S^{ij}}{\partial E_{kl}}\,\mathrm{d}E_{kl} = \mathbb{C}^{ijkl}\,\mathrm{d}E_{kl} \,, \tag{35}$$

where $\mathbb{C} = \mathbb{C}^{ijkl}\mathring{\mathbf{g}}_i \otimes \mathring{\mathbf{g}}_j \otimes \mathring{\mathbf{g}}_k \otimes \mathring{\mathbf{g}}_l$ is the tangent material tensor:

$$\mathbb{C}^{ijkl} = \frac{\partial^2 \psi}{\partial E_{ij}\partial E_{kl}} = 4\frac{\partial^2 \psi}{\partial C_{ij}\partial C_{kl}} \,. \tag{36}$$

Eqs. (34) and (36) are the general formulas from hyperelastic continuum theory. If $C_{33} = g_{33} = 1$ is used for the shell model, the plane stress conditions is, in general, violated, since $S^{33} = 2\frac{\partial \psi}{\partial C_{33}} \neq 0$. Accordingly, the transverse normal deformation C_{33} needs to be determined such that $S^{33} = 0$ is satisfied. This can be done analytically for incompressible materials using the incompressibility condition $J = 1$, or iteratively for compressible materials. Both approaches are shown in detail in the following subsections.

Once the plane stress condition is enforced, it can be used to eliminate the transverse normal strain E_{33} by static condensation of the material tensor:

$$S^{33} = \mathbb{C}^{33\alpha\beta}E_{\alpha\beta} + \mathbb{C}^{3333}E_{33} = 0 \,, \tag{37}$$

implying:

$$E_{33} = -\frac{\mathbb{C}^{33\alpha\beta}}{\mathbb{C}^{3333}}E_{\alpha\beta} \,. \tag{38}$$

The coefficients of the statically condensed material tensor are indicated by $\hat{\mathbb{C}}^{\alpha\beta\gamma\delta}$ and are obtained as:

$$\hat{\mathbb{C}}^{\alpha\beta\gamma\delta} = \mathbb{C}^{\alpha\beta\gamma\delta} - \frac{\mathbb{C}^{\alpha\beta 33}\mathbb{C}^{33\gamma\delta}}{\mathbb{C}^{3333}} \,. \tag{39}$$

5.1. Incompressible materials

To properly deal with incompressibility, the elastic strain energy function $\psi_{el}(\mathbf{C})$ is classically augmented by a constraint term enforcing incompressibility ($J = 1$) via a Lagrange multiplier p, which can be identified as the hydrostatic pressure [50]:

$$\psi = \psi_{el}(\mathbf{C}) - p(J-1) \,. \tag{40}$$

For the shell model, the additional unknown p can be determined and statically condensed using the plane stress condition as shown in the following.

First, the 3D tensors S^{ij} and $\mathbb{C}^{ijkl}$ are formally derived according to Eqs. (34) and (36), considering also p as a function of C_{ij}:

$$S^{ij} = 2\frac{\partial \psi_{el}}{\partial C_{ij}} - 2\frac{\partial p}{\partial C_{ij}}(J-1) - 2p\frac{\partial J}{\partial C_{ij}} \,, \tag{41}$$

$$\mathbb{C}^{ijkl} = 4\frac{\partial^2 \psi_{el}}{\partial C_{ij}\partial C_{kl}} - 4\frac{\partial^2 p}{\partial C_{ij}\partial C_{kl}}(J-1) - 4\frac{\partial p}{\partial C_{ij}}\frac{\partial J}{\partial C_{kl}} - 4\frac{\partial J}{\partial C_{ij}}\frac{\partial p}{\partial C_{kl}} - 4p\frac{\partial^2 J}{\partial C_{ij}\partial C_{kl}} \,, \tag{42}$$

where the derivatives of the Jacobian determinant are obtained as:

$$\frac{\partial J}{\partial C_{ij}} = \frac{1}{2} J \bar{C}^{ij} \,, \tag{43}$$

$$\frac{\partial^2 J}{\partial C_{ij}\partial C_{kl}} = \frac{1}{4} J(\bar{C}^{ij}\bar{C}^{kl} - \bar{C}^{ik}\bar{C}^{jl} - \bar{C}^{il}\bar{C}^{jk}) \,. \tag{44}$$

Substituting Eq. (43) and $J = 1$ into Eq. (41) we can rewrite the plane stress condition as follows:

$$S^{33} = 2\frac{\partial \psi_{el}}{\partial C_{33}} - p\bar{C}^{33} = 0 \,, \tag{45}$$

which can be solved for p:

$$p = 2\frac{\partial \psi_{el}}{\partial C_{33}} C_{33} \,. \tag{46}$$

Accordingly, the derivative of p is obtained as:

$$\frac{\partial p}{\partial C_{ij}} = 2\left(\frac{\partial^2 \psi_{el}}{\partial C_{33}\partial C_{ij}} C_{33} + \frac{\partial \psi_{el}}{\partial C_{33}} \delta^{i3}\delta^{j3}\right), \tag{47}$$

where δ^{ij} is the Kronecker delta. Substituting Eqs. (46)–(47) together with Eqs. (43)–(44) and $J = 1$ into Eqs. (41)–(42), we obtain:

$$S^{ij} = 2\frac{\partial \psi_{el}}{\partial C_{ij}} - 2\frac{\partial \psi_{el}}{\partial C_{33}} C_{33}\bar{C}^{ij}, \tag{48}$$

$$\begin{aligned}\mathbb{C}^{ijkl} = {} & 4\frac{\partial^2 \psi_{el}}{\partial C_{ij}\partial C_{kl}} - 2\frac{\partial \psi_{el}}{\partial C_{33}} C_{33}(\bar{C}^{ij}\bar{C}^{kl} - \bar{C}^{ik}\bar{C}^{jl} - \bar{C}^{il}\bar{C}^{jk}) \\ & - 4\left(\frac{\partial^2 \psi_{el}}{\partial C_{33}\partial C_{ij}} C_{33} + \frac{\partial \psi_{el}}{\partial C_{33}} \delta^{i3}\delta^{j3}\right)\bar{C}^{kl} - 4\bar{C}^{ij}\left(\frac{\partial^2 \psi_{el}}{\partial C_{33}\partial C_{kl}} C_{33} + \frac{\partial \psi_{el}}{\partial C_{33}} \delta^{k3}\delta^{l3}\right).\end{aligned} \tag{49}$$

Eqs. (48)–(49) represent the 3D stress and material tensor for a general incompressible material with $J = 1$ and $S^{33} = 0$ incorporated and p eliminated. For the shell model, only the in-plane components $S^{\alpha\beta}$ and $\mathbb{C}^{\alpha\beta\gamma\delta}$ are considered, where $\bar{C}^{\alpha\beta} = g^{\alpha\beta}$ is used and $C_{33} = J_o^{-2}$ is obtained by Eq. (24). In the incompressible case, the static condensation of E_{33} (see Eq. (39)) can also be performed analytically, as shown in detail in Appendix A. Eventually, the stress tensor and the statically condensed material tensor for the shell with incompressible materials are obtained as follows:

$$S^{\alpha\beta} = 2\frac{\partial \psi_{el}}{\partial C_{\alpha\beta}} - 2\frac{\partial \psi_{el}}{\partial C_{33}} J_o^{-2} g^{\alpha\beta}, \tag{50}$$

$$\begin{aligned}\hat{\mathbb{C}}^{\alpha\beta\gamma\delta} = {} & 4\frac{\partial^2 \psi_{el}}{\partial C_{\alpha\beta}\partial C_{\gamma\delta}} + 4\frac{\partial^2 \psi_{el}}{\partial C_{33}^2} J_o^{-4} g^{\alpha\beta}g^{\gamma\delta} - 4\frac{\partial^2 \psi_{el}}{\partial C_{33}\partial C_{\alpha\beta}} J_o^{-2} g^{\gamma\delta} - 4\frac{\partial^2 \psi_{el}}{\partial C_{33}\partial C_{\gamma\delta}} J_o^{-2} g^{\alpha\beta} \\ & + 2\frac{\partial \psi_{el}}{\partial C_{33}} J_o^{-2}(2g^{\alpha\beta}g^{\gamma\delta} + g^{\alpha\gamma}g^{\beta\delta} + g^{\alpha\delta}g^{\beta\gamma}).\end{aligned} \tag{51}$$

With Eqs. (50)–(51), 3D solid material libraries providing $\dfrac{\partial \psi_{el}}{\partial C_{ij}}$ and $\dfrac{\partial^2 \psi_{el}}{\partial C_{ij}\partial C_{kl}}$ can be directly used for the shell formulation. In case that the components obtained from a material library are provided in Cartesian coordinates rather than curvilinear coordinates, they can be converted to the curvilinear ones by the following formulas, where indices i, j, k, l refer to the curvilinear frame while

a, b, c, d refer to Cartesian coordinates, and where $\mathbf{e}_a$ indicate the global Cartesian base vectors:

$$\frac{\partial \psi_{el}}{\partial C_{ij}} = \frac{\partial \psi_{el}}{\partial C_{ab}} (\mathring{\mathbf{g}}^i \cdot \mathbf{e}_a)(\mathring{\mathbf{g}}^j \cdot \mathbf{e}_b) \,, \tag{52}$$

$$\frac{\partial^2 \psi_{el}}{\partial C_{ij} \partial C_{kl}} = \frac{\partial^2 \psi_{el}}{\partial C_{ab} \partial C_{cd}} (\mathring{\mathbf{g}}^i \cdot \mathbf{e}_a)(\mathring{\mathbf{g}}^j \cdot \mathbf{e}_b)(\mathring{\mathbf{g}}^k \cdot \mathbf{e}_c)(\mathring{\mathbf{g}}^l \cdot \mathbf{e}_d) \,. \tag{53}$$

Neo–Hookean material: In the case of an incompressible Neo–Hookean material, the second derivatives of ψ_{el} vanish and the formulation can be greatly simplified. For that reason, we present it also explicitly in the following. For the Neo–Hookean elastic strain energy function

$$\psi_{el} = \frac{1}{2} \mu \, (I_1 - 3) \,, \tag{54}$$

Eqs. (50) and (51) simply reduce to:

$$S^{\alpha\beta} = \mu \left(\mathring{g}^{\alpha\beta} - J_o^{-2} \, g^{\alpha\beta} \right) \,, \tag{55}$$

$$\hat{\mathbb{C}}^{\alpha\beta\gamma\delta} = \mu \, J_o^{-2} \left(2 g^{\alpha\beta} g^{\gamma\delta} + g^{\alpha\gamma} g^{\beta\delta} + g^{\alpha\delta} g^{\beta\gamma} \right) \,. \tag{56}$$

5.2. Compressible materials

For compressible materials, the plane stress condition $S^{33} = 0$ is satisfied by iteratively solving for C_{33}, using a Newton linearization of the plane stress condition similar to what was presented in [51, 52]:

$$S^{33} + \frac{\partial S^{33}}{\partial C_{33}} \Delta C_{33} = S^{33} + \frac{1}{2} \mathbb{C}^{3333} \Delta C_{33} = 0 \,. \tag{57}$$

From Eq. (57) we obtain the incremental update:

$$\Delta C_{33}^{(I)} = -2 \frac{S_{(I)}^{33}}{\mathbb{C}_{(I)}^{3333}} \,, \tag{58}$$

$$C_{33}^{(I+1)} = C_{33}^{(I)} + \Delta C_{33}^{(I)} \,, \tag{59}$$

where I indicates the iteration step. With the updated $\mathbf{C}$, we compute the updates of $\mathbf{S}(\mathbf{C})$ and $\mathbb{C}(\mathbf{C})$. As an example, let us consider the following compressible Neo–Hookean strain energy function, taken from [53]:

$$\psi = \frac{1}{2} \mu \left(J^{-2/3} \mathrm{tr}(\mathbf{C}) - 3 \right) + \frac{1}{4} K \left(J^2 - 1 - 2 \ln J \right) \,, \tag{60}$$

with μ, K as the shear and bulk moduli. The 3D stress and material tensors are obtained, according to Eqs. (34) and (36), as:

$$S^{ij} = \mu\, J^{-2/3}\left(\mathring{g}^{ij} - \frac{1}{3}\,\mathrm{tr}(\mathbf{C})\,\bar{C}^{ij}\right) + \frac{1}{2}K\,\left(J^2-1\right)\,\bar{C}^{ij}\,, \tag{61}$$

$$\begin{aligned}\mathbb{C}^{ijkl} = {}& \frac{1}{9}\,\mu\, J^{-2/3}\left(\mathrm{tr}(\mathbf{C})\left(2\bar{C}^{ij}\bar{C}^{kl} + 3\bar{C}^{ik}\bar{C}^{jl} + 3\bar{C}^{il}\bar{C}^{jk}\right) - 6\left(\mathring{g}^{ij}\bar{C}^{kl} + \bar{C}^{ij}\mathring{g}^{kl}\right)\right) \\ & + K\left(J^2\,\bar{C}^{ij}\bar{C}^{kl} - \frac{1}{2}(J^2-1)\left(\bar{C}^{ik}\bar{C}^{jl} + \bar{C}^{il}\bar{C}^{jk}\right)\right)\,.\end{aligned} \tag{62}$$

As initial condition we use $C^0_{ij} = g_{ij}$:

$$C^0_{ij} = \begin{pmatrix} g_{11} & g_{12} & 0 \\ g_{21} & g_{22} & 0 \\ 0 & 0 & 1 \end{pmatrix}\,, \tag{63}$$

where the in-plane components remain invariant throughout the iteration, $C_{\alpha\beta} \equiv g_{\alpha\beta}$, and only C^I_{33} is updated. With $C^{(I+1)}_{33}$ obtained according to Eqs. (58)–(59), $\mathrm{tr}(\mathbf{C})^{(I+1)}$ and $J^{(I+1)}$ are updated, and the new values of $S^{ij}_{(I+1)}, \mathbb{C}^{ijkl}_{(I+1)}$ are computed. This procedure is repeated until the plane stress condition is satisfied within a defined tolerance. Finally, the statically condensed material tensor $\hat{\mathbb{C}}$ is computed according to Eq. (39), and only the in-plane components $S^{\alpha\beta}$ and $\hat{\mathbb{C}}^{\alpha\beta\gamma\delta}$ are used for the shell model. As in the incompressible case, arbitrary 3D material models can be used for the shell formulation with this approach.

5.3. Stress resultants

For the shell model, we use stress resultants, obtained by integration through the thickness:

$$n^{\alpha\beta} = \int_{-h/2}^{h/2} S^{\alpha\beta}\mathrm{d}\theta^3\,, \tag{64}$$

$$m^{\alpha\beta} = \int_{-h/2}^{h/2} S^{\alpha\beta}\theta^3\mathrm{d}\theta^3\,, \tag{65}$$

where $n^{\alpha\beta}$ are normal forces and $m^{\alpha\beta}$ are bending moments. For their total differentials, we obtain according to Eqs. (35) and (33):

$$\mathrm{d}n^{\alpha\beta} = \left(\int_{-h/2}^{h/2} \hat{\mathbb{C}}^{\alpha\beta\gamma\delta}\mathrm{d}\theta^3\right)\mathrm{d}\varepsilon_{\gamma\delta} + \left(\int_{-h/2}^{h/2} \hat{\mathbb{C}}^{\alpha\beta\gamma\delta}\,\theta^3\mathrm{d}\theta^3\right)\mathrm{d}\kappa_{\gamma\delta}\,, \tag{66}$$

$$\mathrm{d}m^{\alpha\beta} = \left(\int_{-h/2}^{h/2} \hat{\mathbb{C}}^{\alpha\beta\gamma\delta}\theta^3\mathrm{d}\theta^3\right)\mathrm{d}\varepsilon_{\gamma\delta} + \left(\int_{-h/2}^{h/2} \hat{\mathbb{C}}^{\alpha\beta\gamma\delta}(\theta^3)^2\,\mathrm{d}\theta^3\right)\mathrm{d}\kappa_{\gamma\delta}\,. \tag{67}$$

It should be noted that in Eqs. (66)–(67) only $\hat{\mathbb{C}}^{\alpha\beta\gamma\delta}$ need to be integrated through the thickness, while strain variables are expressed by the midsurface variables $\mathrm{d}\varepsilon_{\gamma\delta}$ and $\mathrm{d}\kappa_{\gamma\delta}$.

6. Variational formulation

We derive the variational formulation from the equilibrium of internal and external virtual work, $\delta W = \delta W^{int} - \delta W^{ext} = 0$, which must hold for any variation (virtual displacement) $\delta\mathbf{u}$, i.e.:

$$\delta W(\mathbf{u}, \delta\mathbf{u}) = D_{\delta\mathbf{u}} W(\mathbf{u}) = 0 \,, \tag{68}$$

where $D_{\delta\mathbf{u}}$ denotes the Gâteaux derivative. For the Kirchhoff–Love shell, internal and external virtual work are defined as:

$$\delta W^{int} = \int_A (\mathbf{n} : \delta\boldsymbol{\varepsilon} + \mathbf{m} : \delta\boldsymbol{\kappa} + \rho\, h\, \ddot{\mathbf{u}} \cdot \delta\mathbf{u})\ \mathrm{d}A \,, \tag{69}$$

$$\delta W^{ext} = \int_A \mathbf{f} \cdot \delta\mathbf{u}\, \mathrm{d}A \,, \tag{70}$$

where $\mathbf{f}$ denotes the external load, $\delta\mathbf{u}$ is a virtual displacement, $\delta\boldsymbol{\varepsilon}$ and $\delta\boldsymbol{\kappa}$ are the corresponding virtual membrane strain and change in curvature, respectively, ρ is the mass density, and $\ddot{\mathbf{u}} = \dfrac{\partial^2\mathbf{u}}{\partial t^2}$ denotes the acceleration. A denotes the midsurface and $\mathrm{d}A = \sqrt{|\mathring{a}_{\alpha\beta}|}\mathrm{d}\theta^1\mathrm{d}\theta^2$ the differential area, both in the reference configuration. This formulation includes the assumption that a differential volume element $\mathrm{d}V$ can be approximated by $\mathrm{d}V \approx h\,\mathrm{d}A$, which is acceptable for thin shells. For static analysis, the acceleration term in Eq. (69) vanishes. In this section we consider the static case only since it includes all terms which are specific for the shell formulation, while in Appendix B we present dynamic formulations using the generalized-α method [54] for time integration.

We perform the linearization of Eqs. (69)–(70) considering a discretized model, such that the Gâteaux derivative in Eq. (68) can be replaced by simple partial derivatives in terms of discrete displacement parameters. The discretized displacement is expressed as:

$$\mathbf{u} = \sum_a^{n_{sh}} N^a \mathbf{u}^a \,, \tag{71}$$

where N^a are the shape functions, with n_{sh} as the total number of shape functions, and $\mathbf{u}^a$ are the nodal displacement vectors with the components u_i^a $(i = 1, 2, 3)$ referring to the global $x-, y-, z-$components. The global degree of freedom number r of a nodal displacement is defined by $r = 3(a-1) + i$, such that $u_r = u_i^a$. The variation with respect to u_r is obtained by the

partial derivative $\partial/\partial u_r$:

$$\frac{\partial \mathbf{u}}{\partial u_r} = N^a \mathbf{e}_i \ . \tag{72}$$

Similar to Eq. (72), the variations of derived variables, such as strains, with respect to u_r can be obtained, which is shown in detail in Appendix C. The variations of δW^{int} and δW^{ext} with respect to u_r yield the vectors of internal and external nodal forces, $\mathbf{F}^{int}$ and $\mathbf{F}^{ext}$, and Eq. (68) becomes:

$$\mathbf{R} = \mathbf{F}^{int} - \mathbf{F}^{ext} = \mathbf{0} \ , \tag{73}$$

with $\mathbf{R}$ as the residual vector and with:

$$F_r^{int} = \int_A \left(\mathbf{n} : \frac{\partial \boldsymbol{\varepsilon}}{\partial u_r} + \mathbf{m} : \frac{\partial \boldsymbol{\kappa}}{\partial u_r} \right) \mathrm{d}A \ , \tag{74}$$

$$F_r^{ext} = \int_A \mathbf{f} \cdot \frac{\partial \mathbf{u}}{\partial u_r} \mathrm{d}A \ . \tag{75}$$

Note that $\mathbf{F}^{ext}$ is the standard load vector obtained by integrating the product of load and shape functions. For the linearization of Eq. (73), we compute the tangential stiffness matrix $\mathbf{K}$, obtained as $K_{rs} = K_{rs}^{int} - K_{rs}^{ext}$:

$$K_{rs}^{int} = \int_A \left(\frac{\partial \mathbf{n}}{\partial u_s} : \frac{\partial \boldsymbol{\varepsilon}}{\partial u_r} + \mathbf{n} : \frac{\partial^2 \boldsymbol{\varepsilon}}{\partial u_r \partial u_s} + \frac{\partial \mathbf{m}}{\partial u_s} : \frac{\partial \boldsymbol{\kappa}}{\partial u_r} + \mathbf{m} : \frac{\partial^2 \boldsymbol{\kappa}}{\partial u_r \partial u_s} \right) \mathrm{d}A \ , \tag{76}$$

$$K_{rs}^{ext} = \int_A \frac{\partial \mathbf{f}}{\partial u_s} \cdot \frac{\partial \mathbf{u}}{\partial u_r} \mathrm{d}A \ , \tag{77}$$

where K_{rs}^{ext} is to be considered only for displacement-dependent loads $\mathbf{f} = \mathbf{f}(\mathbf{u})$. Note that in cases where $\mathbf{K}^{ext}$ is difficult to compute, it is also possible to neglect its contribution, which means that the tangential stiffness matrix is only approximated. Nevertheless, the method converges to the correct solution as long as the residual $\mathbf{R}$ is computed correctly. Finally, we get the linearized equation system which is solved for the incremental displacement vector $\Delta\mathbf{u}$:

$$\mathbf{K}\,\Delta\mathbf{u} = -\mathbf{R} \ . \tag{78}$$

Note that with a slight abuse of notation, we use $\mathbf{u}$ for also for the vector of discrete nodal displacements.

7. Isogeometric discretization and implementation details

Eqs. (74)–(78) represent a general displacement-based formulation for hyperelastic Kirchhoff–Love shells. Due to the second derivatives contained in the curvatures, C^1 continuity or higher is required for the shape functions, which makes IGA an ideal discretization approach for this formulation. The basics on IGA have been presented in detail in numerous papers and we do not repeat them here again, but refer to [55, 56] for an introduction to NURBS, to [17, 24] for details on IGA, and to [27, 57] for its application to geometrically nonlinear Kirchhoff–Love shell analysis. In the present paper, we employ both NURBS and T-splines discretizations. Analysis with T-splines is based on Bézier extraction [58], such that the integration at element level is performed in the same way as for classical finite elements while the T-spline structure is recovered during assembly into the global matrices.

The continuity properties of the isogeometric basis functions allow a straightforward implementation of the presented theory without the need for rotational degrees of freedom and with curvatures computed exactly. The natural coordinates ξ, η of the isogeometric parametrization are identified as the shell coordinates θ^1, θ^2 such that all the formulations presented in the previous sections for the theoretical model can be implemented one-to-one, without the need for any coordinate transformation. Rotational boundary conditions, such as clamped boundaries or symmetry conditions are imposed via the displacements of the second row of control points from the boundary, as described in [27]. The same approach is also used for imposing C^1 continuity between patches in the case of multipatch structures, see [27]. We emphasize that this approach of patch coupling works perfectly well also for large deformations and rigid body rotations, but it is restricted to smooth patch connections. For coupling arbitrary patch connections, including also kinks and folds, the bending strip method [59] can be employed. Alternatively, penalty formulations as in [42, 60] or a Nitsche formulation as in [61] may be used for patch coupling.

For an efficient implementation, we express all relevant vectors and tensors in Voigt notation:

$$\overline{\mathbf{n}} = \begin{pmatrix} n^{11} \\ n^{22} \\ n^{12} \end{pmatrix}, \qquad \overline{\mathbf{m}} = \begin{pmatrix} m^{11} \\ m^{22} \\ m^{12} \end{pmatrix}, \qquad \overline{\boldsymbol{\varepsilon}} = \begin{pmatrix} \varepsilon_{11} \\ \varepsilon_{22} \\ 2\,\varepsilon_{12} \end{pmatrix}, \qquad \overline{\boldsymbol{\kappa}} = \begin{pmatrix} \kappa_{11} \\ \kappa_{22} \\ 2\,\kappa_{12} \end{pmatrix}, \tag{79}$$

with the material tensor represented as a 3×3 material matrix:

$$\overline{\mathbf{D}} = \begin{pmatrix} \hat{\mathbb{C}}^{1111} & \hat{\mathbb{C}}^{1122} & \hat{\mathbb{C}}^{1112} \\ & \hat{\mathbb{C}}^{2222} & \hat{\mathbb{C}}^{2212} \\ \textit{symm.} & & \hat{\mathbb{C}}^{1212} \end{pmatrix}. \tag{80}$$

Furthermore, we introduce the following "thickness-integrated" material matrices:

$$\overline{\mathbf{D}}^0 = \int_{-h/2}^{h/2} \overline{\mathbf{D}}\, \mathrm{d}\theta^3 \,, \qquad \overline{\mathbf{D}}^1 = \int_{-h/2}^{h/2} \theta^3 \overline{\mathbf{D}}\, \mathrm{d}\theta^3 \,, \qquad \overline{\mathbf{D}}^2 = \int_{-h/2}^{h/2} \left(\theta^3\right)^2 \overline{\mathbf{D}}\, \mathrm{d}\theta^3 \,, \tag{81}$$

such that we can rewrite Eqs. (66)–(67) as:

$$\mathrm{d}\overline{\mathbf{n}} = \overline{\mathbf{D}}^0\, \mathrm{d}\overline{\boldsymbol{\varepsilon}} + \overline{\mathbf{D}}^1\, \mathrm{d}\overline{\boldsymbol{\kappa}} \,, \tag{82}$$

$$\mathrm{d}\overline{\mathbf{m}} = \overline{\mathbf{D}}^1\, \mathrm{d}\overline{\boldsymbol{\varepsilon}} + \overline{\mathbf{D}}^2\, \mathrm{d}\overline{\boldsymbol{\kappa}} \,. \tag{83}$$

Now we can express the internal forces (74) and stiffness matrix (76) as:

$$F_r^{int} = \int_A \left(\overline{\mathbf{n}}^T \frac{\partial \overline{\boldsymbol{\varepsilon}}}{\partial u_r} + \overline{\mathbf{m}}^T \frac{\partial \overline{\boldsymbol{\kappa}}}{\partial u_r} \right) \mathrm{d}A \,, \tag{84}$$

$$K_{rs} = \int_A \left(\left(\overline{\mathbf{D}}^0 \frac{\partial \overline{\boldsymbol{\varepsilon}}}{\partial u_s} + \overline{\mathbf{D}}^1 \frac{\partial \overline{\boldsymbol{\kappa}}}{\partial u_s} \right)^T \frac{\partial \overline{\boldsymbol{\varepsilon}}}{\partial u_r} + \overline{\mathbf{n}}^T \frac{\partial^2 \overline{\boldsymbol{\varepsilon}}}{\partial u_r \partial u_s} + \left(\overline{\mathbf{D}}^1 \frac{\partial \overline{\boldsymbol{\varepsilon}}}{\partial u_s} + \overline{\mathbf{D}}^2 \frac{\partial \overline{\boldsymbol{\kappa}}}{\partial u_s} \right)^T \frac{\partial \overline{\boldsymbol{\kappa}}}{\partial u_r} + \overline{\mathbf{m}}^T \frac{\partial^2 \overline{\boldsymbol{\kappa}}}{\partial u_r \partial u_s} \right) \mathrm{d}A \,. \tag{85}$$

This formulation is computationally efficient since the thickness integration is performed only for the stress and material variables, while the linearization of the strains, which represents the large part of the computational load, is performed only on the midsurface. The linearization of $\boldsymbol{\varepsilon}$ and $\boldsymbol{\kappa}$ with respect to u_r, u_s are presented in detail in Appendix C.

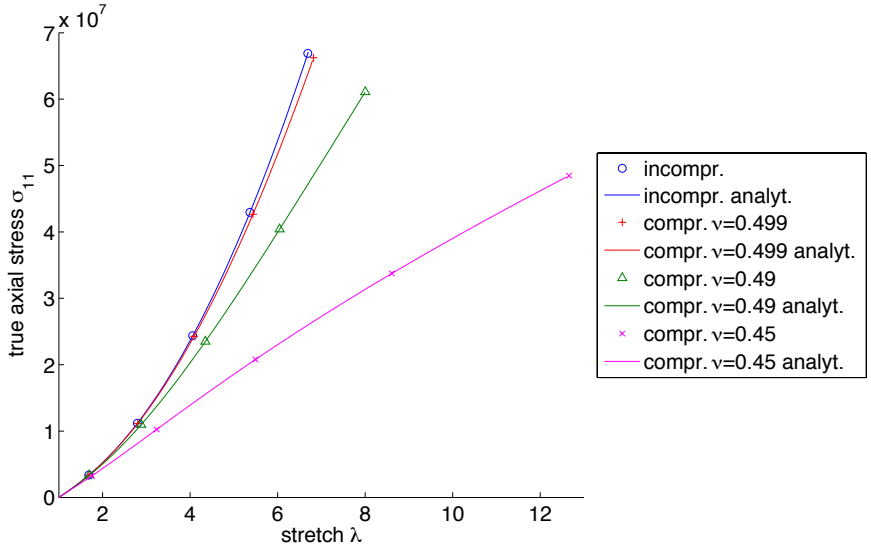

Figure 1: Uniaxial tensile test. Stretch-stress curve for different Neo–Hookean materials.

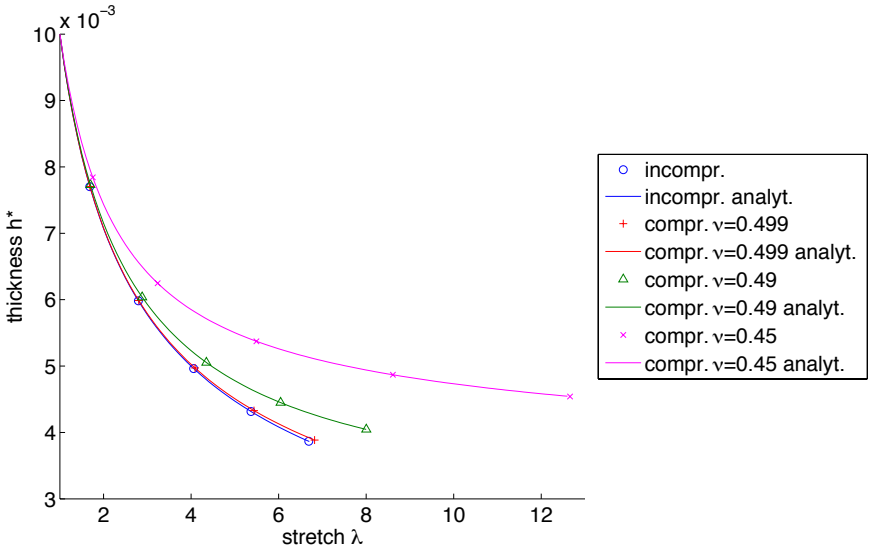

Figure 2: Uniaxial tensile test. Stretch-thickness curve for different Neo–Hookean materials.

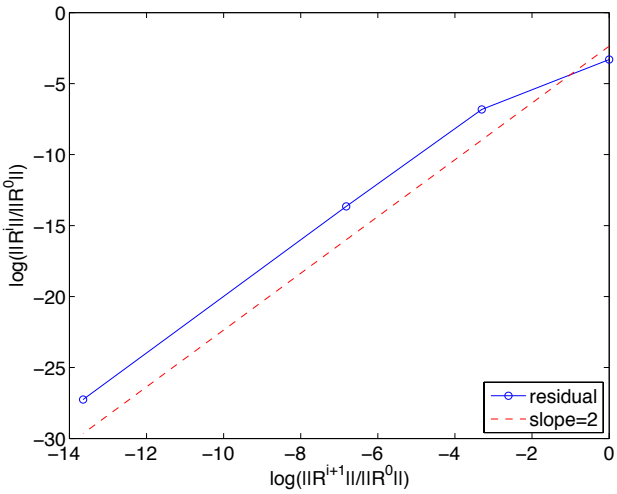

Figure 3: Uniaxial tensile test. Convergence diagram for the last load step of the compressible case with $\nu = 0.499$ (note that R^i indicates the residual of the i^{th} iteration).

8. Numerical tests

We present several numerical tests using different compressible, nearly-incompressible, and incompressible materials. The tests include benchmark examples with analytical solutions or reference solutions from literature, as well as the application to structural dynamics simulations of a bioprosthetic heart valve (BHV).

8.1. Uniaxial tensile test

As a first example, we simulate a simple uniaxial tensile test, for which analytical solutions can be derived. A square membrane of dimensions 1 m $\times$ 1 m $\times$ 0.01 m is subjected to uniaxial

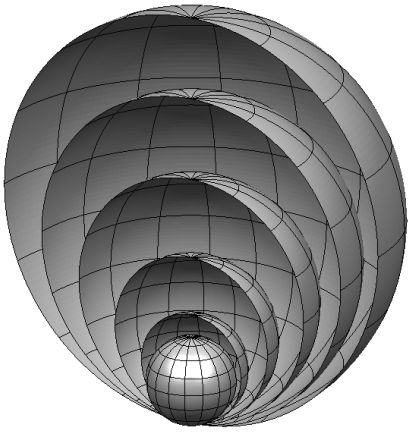

Figure 4: Inflation of a balloon. Undeformed geometry (full sphere) and deformed geometries of every other load step (half spheres).

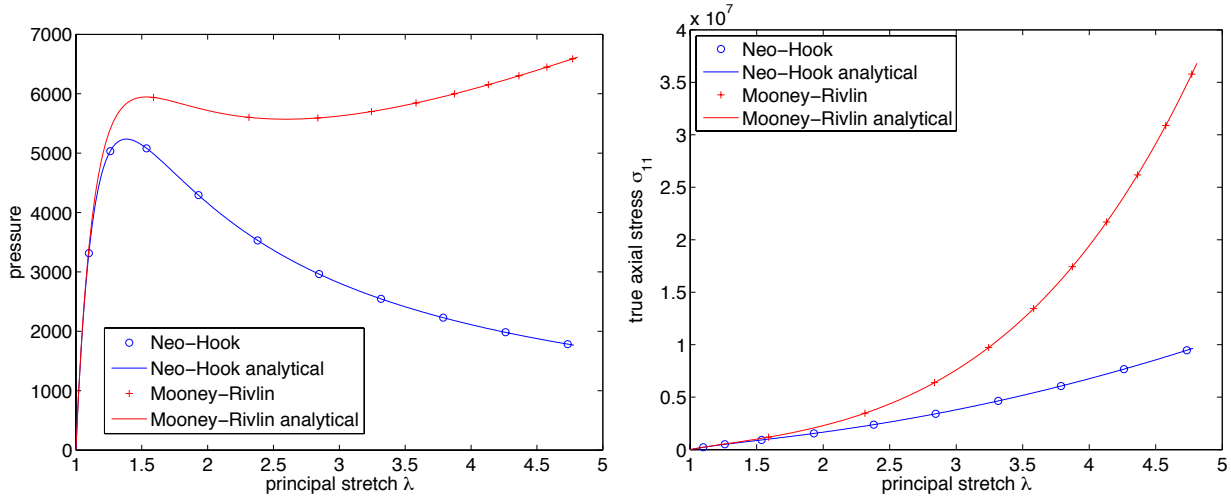

Figure 5: Inflation of a ballon. Stretch-pressure (left) and stretch-stress (right) curves for incompressible Neo-Hook and Mooney Rivlin materials.

tensile loading and different constitutive models are employed. Firstly, we consider an incompressible Neo–Hookean material as given in Eq. (54). The analytical solution for the stress-stretch relationship in this case is:

$$\sigma = \mu \left(\lambda^2 - \lambda^{-1} \right) , \tag{86}$$

with $\sigma = \sigma^{11}$ and $\lambda = \lambda_1$, $\lambda_2 = \lambda_3 = \sqrt{1/\lambda}$.

Secondly, we consider the compressible Neo–Hookean material presented in Eq. (60). The

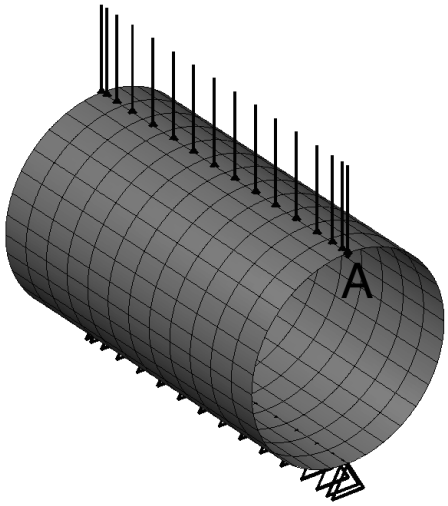

Figure 6: Pinched cylinder problem setup.

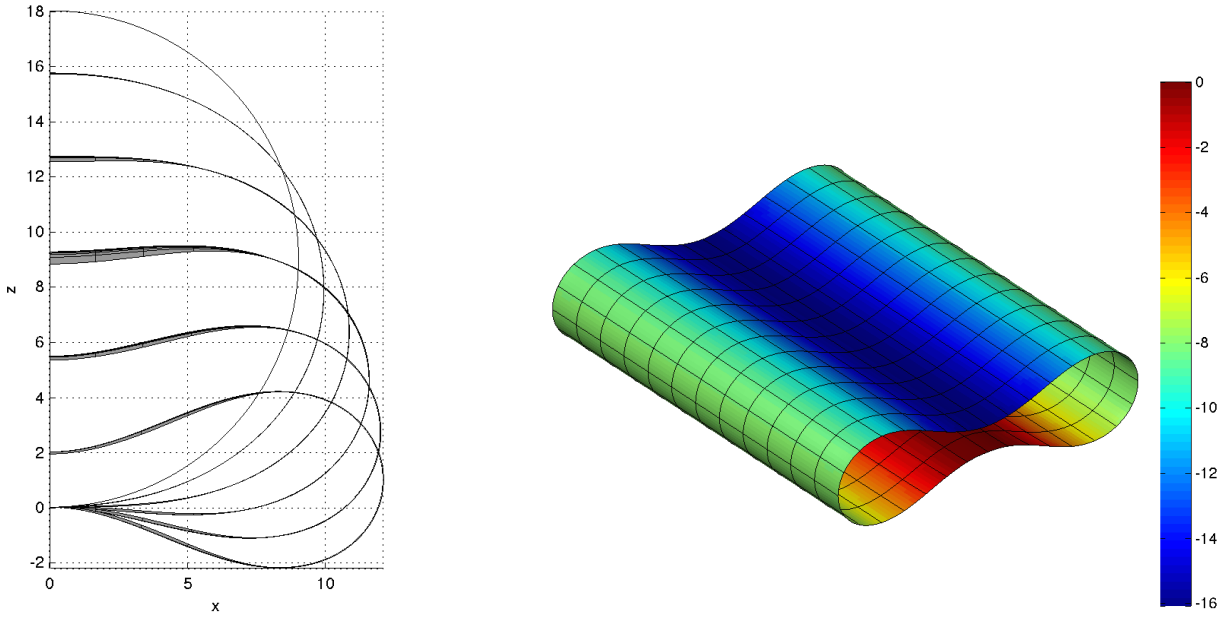

(a) (b)

Figure 7: Pinched cylinder. Deformation of the half-system at every single load step in front view (a), and contour plot of the final deformed configuration (total system assembled for visualization) with the colors indicating the vertical displacement in *cm* (b).

analytical solution is obtained by solving the equation $\sigma^{33} = 0$, which becomes:

$$-\frac{1}{3}\mu J^{-5/3}\left(\lambda^2 - J\lambda^{-1}\right) + \frac{1}{2}K\left(\lambda - \lambda^{-1}\right) = 0\,. \tag{87}$$

Eq. (87) is solved for J, which is then substituted into:

$$\sigma = \mu J^{-5/3} \left(\lambda^2 - J\lambda^{-1} \right) , \tag{88}$$

with $\sigma = \sigma^{11}$ and $\lambda = \lambda_1$, $\lambda_2 = \lambda_3 = \sqrt{J/\lambda}$.

The problem is solved numerically by one cubic shell element for both the incompressible and the compressible cases. As material parameters, we use $\mu = 1.5 \times 10^6$ N/m^2 in all cases, while different values for the Poisson's ratio $\nu = \{0.45, 0.49, 0.499\}$ are used for the compressible formulation, with $K = 2\mu(1+\nu)/(3-6\nu)$. In Figure 1, the stretch-stress curves for the different models are depicted. A perfect agreement with the analytical solutions can be observed for all cases. Furthermore, we use the relation $\lambda_3 = \sqrt{C_{33}}$ in order to compute the deformed thickness, $h^* = \lambda_3 h$. The results are plotted in Figure 2, where, again, a perfect agreement with the analytical solutions can be observed. In order to investigate the consistency of the linearization, we also check for the convergence rate of the solution. Exemplarily, we plot in Figure 3 the convergence of the last load step for the compressible Neo–Hookean material with $\nu = 0.499$. As can be seen, the expected quadratic convergence is correctly obtained.

In addition, we have performed this test with all material models used in the following examples. In all cases, a perfect match with the analytical solutions as in Figures 1 and 2 and quadratic convergence as in Figure 3 have been observed.

8.2. Inflation of a balloon

As a second example, we study the inflation of a balloon, which represents a biaxial membrane stress state, and for which analytical solutions are given in [50]. For this test, we consider an incompressible Neo–Hookean material (54) as well as an incompressible Mooney–Rivlin material defined by:

$$\psi_{el} = \frac{1}{2} c_1 \left(I_1 - 3 \right) - \frac{1}{2} c_2 \left(I_2 - 3 \right) , \tag{89}$$

with $c_1 = \mu_1/2, c_2 = -\mu_2/2$ and $\mu_1 - \mu_2 = \mu$. We compute both the stress $\sigma = \sigma_{11} = \sigma_{22}$ and the internal pressure p_i as functions of the stretch $\lambda = \lambda_1 = \lambda_2$, for which the analytical solutions are given as:

$$\text{Neo–Hookean:} \qquad \sigma = \mu(\lambda^2 - \lambda^4) , \tag{90}$$

$$p_i = 2tR^{-1}\mu(\lambda^{-1} - \lambda^{-7}) , \tag{91}$$

$$\text{Mooney–Rivlin:} \qquad \sigma = \mu_1(\lambda^2 - \lambda^4) + \mu_2(\lambda^{-2} - \lambda^{-4}) , \tag{92}$$

$$p_i = 2tR^{-1} \left(\mu_1(\lambda^{-1} - \lambda^{-7}) + \mu_2(\lambda^{-5} - \lambda) \right) , \tag{93}$$

with R as the radius and t as the thickness of the sphere in the undeformed configuration. The adopted geometrical and material parameters are $R = 10.0$ m, $t = 0.1$ m, $\mu = 4.225 \times 10^5$ N/m^2, $c_1 = 0.4375\mu$, and $c_2 = 0.0625\mu$ ($c_1/c_2 = 7$), see [50]. We model the whole sphere with 8×16 cubic elements. In Figure 4 the undeformed geometry (full sphere) and the deformed geometries of every other load step (half spheres) are depicted, while Figure 5 shows the stretch-pressure and stretch-stress curves, where a perfect agreement with the analytical solutions can be observed for both materials.

8.3. Pinching of a cylinder

This bending-dominated problem was firstly presented in [4] and was subsequently studied in [3, 8, 9]. A cylinder with radius $R = 9$ cm, length $L = 30$ cm, and thickness $t = 0.2$ cm is supported at the bottom and subjected to a line load at the top, as shown in Figure 6. A compressible Neo–Hookean material is used, defined by the following strain energy function:

$$\psi = \frac{\mu}{2}\left(\mathrm{tr}(\mathbf{C}) - 3\right) - \mu \ln\left(\sqrt{\det(\mathbf{C})}\right) + \frac{\Lambda}{4}\left(\det(\mathbf{C}) - 1 - 2\ln\left(\sqrt{\det(\mathbf{C})}\right)\right) , \tag{94}$$

with $\mu = 60$ kN/mm^2 and $\Lambda = 240$ kN/mm^2 as the Lamé constants. A uniform line load is applied such that the vertical displacement of point A on the top of the rim is 16 cm. Due to symmetry, we model only half of the cylinder and discretize it with 16×12 quartic elements. For imposing symmetry conditions, the x-displacements (perpendicular to the symmetry plane) of the control points at the top are blocked. Furthermore, rotations around the y-axis in the symmetry plane are prevented by constraining the z-displacement of the second row of control points both at the top and the bottom to be equal to the one of the neighboring control points (first row at top and bottom) as described in [57]. Figure 7(a) depicts the deformation for all load steps while Figure 7(b) shows a contour plot of the final deformed configuration with the colors indicating the vertical displacement. The total load corresponding to the displacement $u(A) = 16$ cm is obtained as $F = 34.86$ kN which is in good agreement with the results from literature ranging between 34.59 kN and 35.47 kN (a detailed overview of these results can be found in [9]).

8.4. Dynamic simulation of a bioprosthetic heart valve

In this section, we consider a dynamic simulation of pericardial BHV function over a complete cardiac cycle with prescribed physiological transvalvular pressure load. This type of BHV is fabricated from bovine pericardium sheets that are chemically treated after being die-cut and mounted onto a metal frame to form the leaflets. The strong stiffening effect of the tissue observed at higher loadings motivates the use of an exponential function for describing the mechanical behavior of

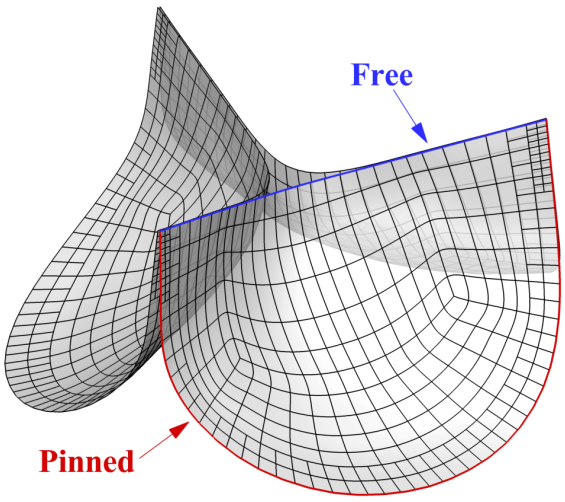

Figure 8: The trileaflet T-spline BHV model. The pinned boundary condition is applied to the leaflet attachment edge.

the leaflets [62, 63]. In this study, we choose the following strain energy function

$$\psi_{el} = \frac{c_0}{2}(I_1 - 3) + \frac{c_1}{2}\left(e^{c_2(I_1-3)^2} - 1\right) , \tag{95}$$

which is an exponential-type isotropic model with a Neo–Hookean component [64], with $c_0 = 0.2$ MPa, $c_1 = 0.05$ MPa, and $c_3 = 100$. The order of magnitude of the parameters is chosen to give a comparable stiffness to the material models used in [64–66].

The geometry of the trileaflet BHV is modeled using three cubic T-spline surfaces, one for each leaflet, as shown in Figure 8, and is based on the 23-mm NURBS model used in [67, 68]. T-splines enable local refinement and coarsening [19, 69], which is more flexible so that the new parameterization of the leaflet avoids the small, degenerated NURBS elements used in [67] near the commissure points. The T-spline surfaces were generated using the Autodesk T-Splines Plug-in for Rhino [70, 71]. The Bézier extraction data files can be obtained using the same tool.

The T-spline mesh is comprised of a total of 1,452 Bézier elements and 1,329 T-spline control points. The thickness of the leaflets is 0.0386 cm and the density is 1.0 g/cm^3. We model the transvalvular pressure (i.e., pressure difference between left ventricle and aorta) with the traction $-P(t)\mathbf{a}_3$, where $P(t)$ is the pressure difference at time t, taken from the profile used in [66] and reproduced in Figure 9, and $\mathbf{a}_3$ is the surface normal pointing from the aortic to the ventricular side of each leaflet. The duration of a single cardiac cycle is 0.76 s. As in the computations of [66, 67], we use damping to model the viscous and inertial resistance of the surrounding fluid. The damping matrix $\mathbf{C}_d$ (see Eq. (B.1)) can be obtained by

$$(C_d)_{rs} = c_d \int_{A^*} \frac{\partial \mathbf{u}}{\partial u_s} \cdot \frac{\partial \mathbf{u}}{\partial u_r} \mathrm{d}A , \tag{96}$$

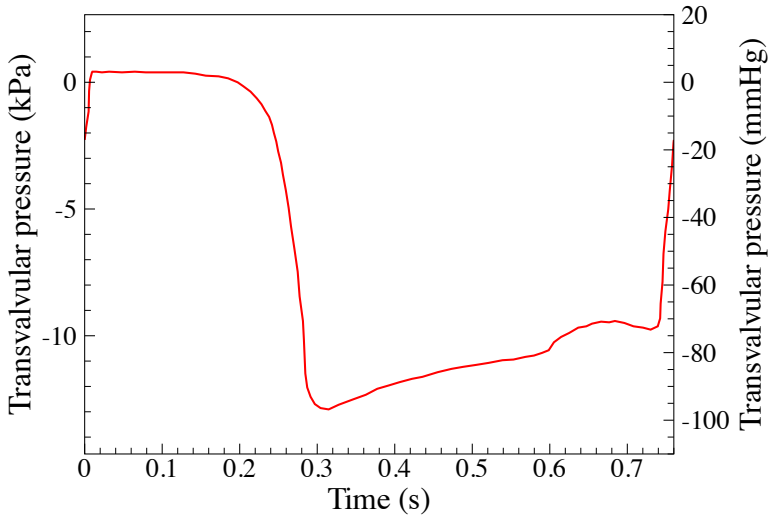

Figure 9: Transvalvular pressure applied to the leaflets as a function of time. The duration of a single cardiac cycle is 0.76 s.

where A^* is the midsurface in the current configuration and $c_d = 80$ g/(cm^2 s) is used in this work. This value of c_d is selected to ensure that the valve opens at a physiologically reasonable time scale when the given pressure is applied. Note that the damping matrix defined in Eq. (96) is a function of the current configuration and, accordingly, needs to be linearized in order to compute the consistent tangent stiffness matrix. In our computations, we use an approximated tangent stiffness matrix by neglecting this term as well as the stiffness contribution corresponding to the pressure load. The time-step size used in the dynamic simulation is 0.0001 s and the pinned boundary condition is applied to the leaflet attachment edge as shown in Figure 8. The penalty-based contact algorithm proposed in [67] is used in the simulation. We compute for several cycles until reaching a time-periodic solution.

The deformation and maximum in-plane principal strain distribution of the leaflets at several points in the cardiac cycle is shown in Figure 10. The opening is qualitatively similar to that computed by [67], who used a St. Venant–Kirchhoff material with $E = 10^7$ dyn/cm^2 and $\nu = 0.45$, and quadratic B-splines to model the BHV. The pressurized diastolic state, however, exhibits less sagging of the belly region compared with that reported in [67] because the material model used in this study includes the exponential stiffening under strain.

9. Conclusion

We have presented Kirchhoff–Love shell formulations for compressible and incompressible nonlinear hyperelastic materials. The shell kinematics are completely described by the midsurface metric and curvature variables while the thickness stretch is statically condensed using the plane stress condition. This condensation is done iteratively for compressible materials and analytically

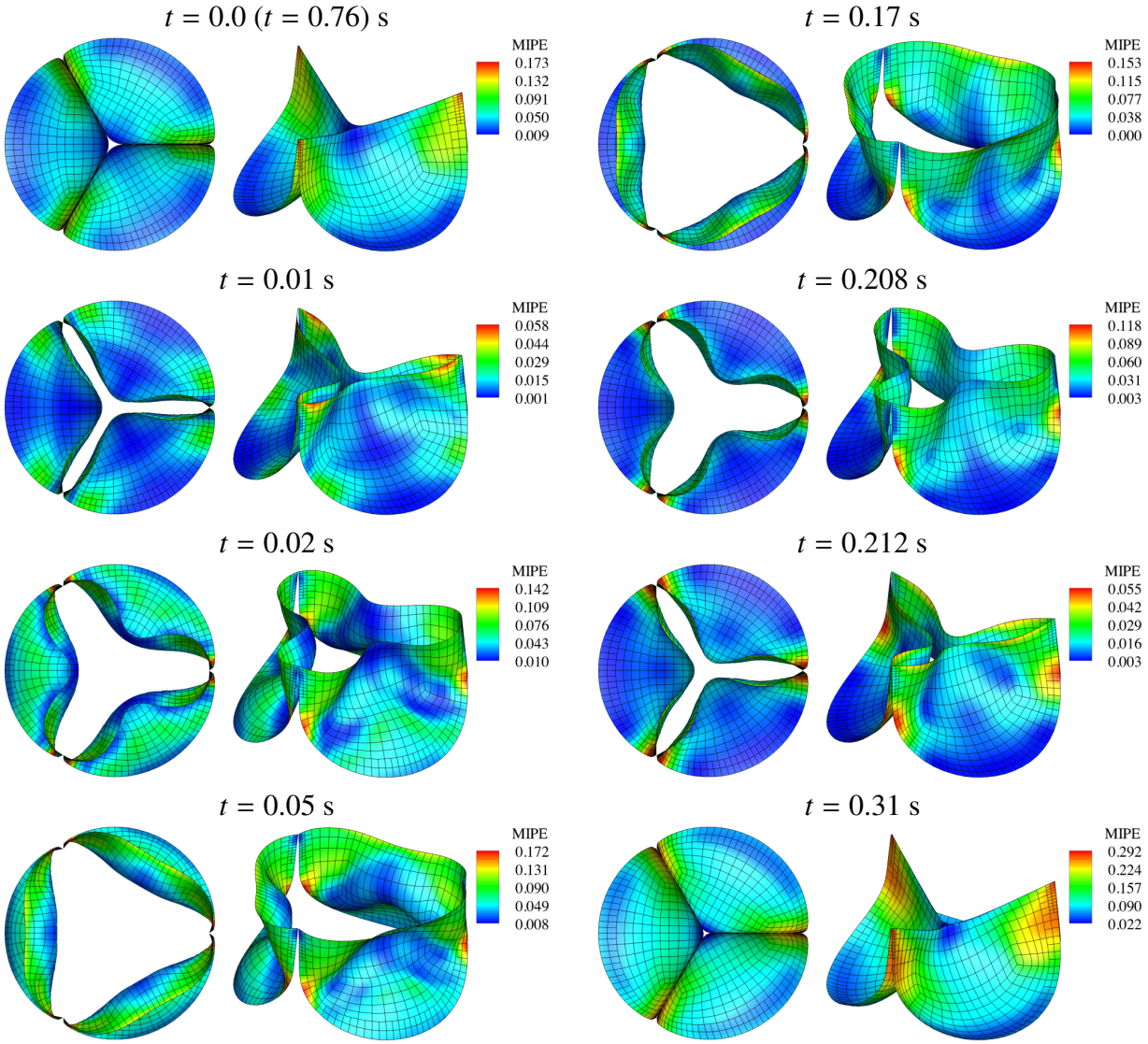

Figure 10: Deformations of the valve from a cycle of the dynamic computation, colored by maximum in-plane principal Green-Lagrange strain (MIPE, the largest eigenvalue of **E**), evaluated on the aortic side of the leaflet. Note the different scale for each time. Time is synchronized with Figure 9. The solution at $t = 0$ s comes from the preceding cycle and is not the stress-free configuration.

for incompressible materials, while both approaches are derived in such a manner that general 3D constitutive models can be directly used for the shell formulation. We show the detailed derivation of the proposed formulation which can be used in combination with any discretization technique providing C^1 continuity. We adopt isogeometric discretizations, in particular, NURBS and T-splines, where control point displacements are the only degrees of freedom. We have successfully tested the method on a series of benchmark problems for different compressible (including nearly incompressible) and incompressible materials. Furthermore, we have applied it to structural dynamics simulations of a bioprosthetic heart valve. The extension to anisotropic materials is planned as future work. Such an extension should be rather straightforward but needs to include local coordinate transformations and, therefore, will loose some of the nice features that we want to highlight in the present formulation. Furthermore, we plan the extension of the present formulation to other nonlinear constitutive models like plasticity and viscoelasticity.

Acknowledgements

J. Kiendl and A. Reali were partially supported by the European Research Council through the FP7 Ideas Starting Grant No. 259229 *ISOBIO*. M.-C. Hsu and M.C.H. Wu are partially supported by the Office of Energy Efficiency and Renewable Energy (EERE), U.S. Department of Energy, under Award Number DE-EE0006737. We thank the Texas Advanced Computing Center (TACC) at the University of Texas at Austin for providing HPC resources that have contributed to the research results reported in this paper. These supports are gratefully acknowledged.

Appendix A. Static condensation of E_{33} for incompressible materials

The statically condensed material tensor coefficients $\hat{\mathbb{C}}^{\alpha\beta\gamma\delta}$ are generally obtained according to Eq. (39):

$$\hat{\mathbb{C}}^{\alpha\beta\gamma\delta} = \mathbb{C}^{\alpha\beta\gamma\delta} - \frac{\mathbb{C}^{\alpha\beta 33}\mathbb{C}^{33\gamma\delta}}{\mathbb{C}^{3333}} \,. \tag{A.1}$$

With $\mathbb{C}^{ijkl}$ as defined in (49) and repeated here for convenience:

$$\begin{aligned}\mathbb{C}^{ijkl} &= 4\frac{\partial^2\psi_{el}}{\partial C_{ij}\partial C_{kl}} - 2\frac{\partial\psi_{el}}{\partial C_{33}}C_{33}(\bar{C}^{ij}\bar{C}^{kl} - \bar{C}^{ik}\bar{C}^{jl} - \bar{C}^{il}\bar{C}^{jk}) \\ &\quad - 4\left(\frac{\partial^2\psi_{el}}{\partial C_{33}\partial C_{ij}}C_{33} + \frac{\partial\psi_{el}}{\partial C_{33}}\delta^{i3}\delta^{j3}\right)\bar{C}^{kl} - 4\bar{C}^{ij}\left(\frac{\partial^2\psi_{el}}{\partial C_{33}\partial C_{kl}}C_{33} + \frac{\partial\psi_{el}}{\partial C_{33}}\delta^{k3}\delta^{l3}\right) \,,\end{aligned} \tag{A.2}$$

we compute explicitly the single terms of (A.1):

$$\begin{aligned}\mathbb{C}^{\alpha\beta\gamma\delta} &= 4\frac{\partial^2\psi_{el}}{\partial C_{\alpha\beta}\partial C_{\gamma\delta}} - 2\frac{\partial\psi_{el}}{\partial C_{33}}C_{33}(\bar{C}^{\alpha\beta}\bar{C}^{\gamma\delta} - \bar{C}^{\alpha\gamma}\bar{C}^{\beta\delta} - \bar{C}^{\alpha\delta}\bar{C}^{\beta\gamma}) \\ &\quad - 4\frac{\partial^2\psi_{el}}{\partial C_{33}\partial C_{\alpha\beta}}C_{33}\bar{C}^{\gamma\delta} - 4\bar{C}^{\alpha\beta}\frac{\partial^2\psi_{el}}{\partial C_{33}\partial C_{\gamma\delta}}C_{33} \,,\end{aligned} \tag{A.3}$$

and:

$$\begin{aligned}\mathbb{C}^{\alpha\beta 33} &= 4\frac{\partial^2\psi_{el}}{\partial C_{\alpha\beta}\partial C_{33}} - 2\frac{\partial\psi_{el}}{\partial C_{33}}C_{33}(\bar{C}^{\alpha\beta}\bar{C}^{33}) - 4\left(\frac{\partial^2\psi_{el}}{\partial C_{33}\partial C_{\alpha\beta}}C_{33}\right)\bar{C}^{33} - 4\bar{C}^{\alpha\beta}\left(\frac{\partial^2\psi_{el}}{\partial C_{33}^2}C_{33} + \frac{\partial\psi_{el}}{\partial C_{33}}\right) \\ &= -\bar{C}^{\alpha\beta}\left(6\frac{\partial\psi_{el}}{\partial C_{33}} + 4\frac{\partial^2\psi_{el}}{\partial C_{33}^2}C_{33}\right) \,.\end{aligned} \tag{A.4}$$

Due to symmetry, $\mathbb{C}^{33\gamma\delta}$ is obtained directly from (A.4):

$$\mathbb{C}^{33\gamma\delta} = -\bar{C}^{\gamma\delta}\left(6\frac{\partial\psi_{el}}{\partial C_{33}} + 4\frac{\partial^2\psi_{el}}{\partial C_{33}^2}C_{33}\right) \,. \tag{A.5}$$

Furthermore, we compute:

$$\begin{aligned}\mathbb{C}^{3333} &= 4\frac{\partial^2\psi_{el}}{\partial C_{33}^2} + 2\frac{\partial\psi_{el}}{\partial C_{33}}C_{33}(\bar{C}^{33})^2 - 4\left(\frac{\partial^2\psi_{el}}{\partial C_{33}^2}C_{33} + \frac{\partial\psi_{el}}{\partial C_{33}}\right)\bar{C}^{33} - 4\bar{C}^{33}\left(\frac{\partial^2\psi_{el}}{\partial C_{33}^2}C_{33} + \frac{\partial\psi_{el}}{\partial C_{33}}\right) \\ &= -\bar{C}^{33}\left(6\frac{\partial\psi_{el}}{\partial C_{33}} + 4\frac{\partial^2\psi_{el}}{\partial C_{33}^2}C_{33}\right) \,.\end{aligned} \tag{A.6}$$

With (A.4)–(A.6) we obtain:

$$\frac{\mathbb{C}^{\alpha\beta 33}\mathbb{C}^{33\gamma\delta}}{\mathbb{C}^{3333}} = -\bar{C}^{\alpha\beta}\bar{C}^{\gamma\delta}\left(6\frac{\partial\psi_{el}}{\partial C_{33}}C_{33} + 4\frac{\partial^2\psi_{el}}{\partial C_{33}^2}C_{33}^2\right) . \tag{A.7}$$

Substituting (A.3) and (A.7) into (A.1) yields:

$$\begin{aligned}\hat{\mathbb{C}}^{\alpha\beta\gamma\delta} = {} & 4\frac{\partial^2\psi_{el}}{\partial C_{\alpha\beta}\partial C_{\gamma\delta}} + 4\frac{\partial^2\psi_{el}}{\partial C_{33}^2}C_{33}^2\bar{C}^{\alpha\beta}\bar{C}^{\gamma\delta} - 4\frac{\partial^2\psi_{el}}{\partial C_{33}\partial C_{\alpha\beta}}C_{33}\bar{C}^{\gamma\delta} - 4\bar{C}^{\alpha\beta}\frac{\partial^2\psi_{el}}{\partial C_{33}\partial C_{\gamma\delta}}C_{33} \\ & + 2\frac{\partial\psi_{el}}{\partial C_{33}}C_{33}(2\bar{C}^{\alpha\beta}\bar{C}^{\gamma\delta} + \bar{C}^{\alpha\gamma}\bar{C}^{\beta\delta} + \bar{C}^{\alpha\delta}\bar{C}^{\beta\gamma}) .\end{aligned} \tag{A.8}$$

Finally, we substitute $\bar{C}^{\alpha\beta} = g^{\alpha\beta}$ and $C_{33} = J_o^{-2}$ into (A.8) and obtain:

$$\begin{aligned}\hat{\mathbb{C}}^{\alpha\beta\gamma\delta} = {} & 4\frac{\partial^2\psi_{el}}{\partial C_{\alpha\beta}\partial C_{\gamma\delta}} + 4\frac{\partial^2\psi_{el}}{\partial C_{33}^2}J_o^{-4}g^{\alpha\beta}g^{\gamma\delta} - 4\frac{\partial^2\psi_{el}}{\partial C_{33}\partial C_{\alpha\beta}}J_o^{-2}g^{\gamma\delta} - 4\frac{\partial^2\psi_{el}}{\partial C_{33}\partial C_{\gamma\delta}}J_o^{-2}g^{\alpha\beta} \\ & + 2\frac{\partial\psi_{el}}{\partial C_{33}}J_o^{-2}(2g^{\alpha\beta}g^{\gamma\delta} + g^{\alpha\gamma}g^{\beta\delta} + g^{\alpha\delta}g^{\beta\gamma}) .\end{aligned} \tag{A.9}$$

Appendix B. Dynamic formulations with generalized-α method

For the dynamic problem, the semi-discrete residual form of the nonlinear problem reads as:

$$\mathbf{R} = \mathbf{M}\ddot{\mathbf{u}} + \mathbf{C}_d\dot{\mathbf{u}} + \mathbf{F}^{int} - \mathbf{F}^{ext} = \mathbf{0} , \tag{B.1}$$

where $\dot{\mathbf{u}}$ is the velocity and $\ddot{\mathbf{u}}$ the acceleration. $\mathbf{M}$ is the standard mass matrix, obtained by:

$$M_{rs} = \rho\, h \int_A \frac{\partial\mathbf{u}}{\partial u_s}\cdot\frac{\partial\mathbf{u}}{\partial u_r}\mathrm{d}A , \tag{B.2}$$

while $\mathbf{C}_d$ is the viscous damping matrix [72].

In the generalized α-method [24, 54], all variables are interpolated at a time instant between two discrete time steps t_n and t_{n+1} by the interpolation factors α_f, α_m, which is indicated by a subscript α in the following:

$$\mathbf{u}_\alpha = \alpha_f\mathbf{u}_{n+1} + (1-\alpha_f)\mathbf{u}_n , \tag{B.3}$$

$$\dot{\mathbf{u}}_\alpha = \alpha_f\dot{\mathbf{u}}_{n+1} + (1-\alpha_f)\dot{\mathbf{u}}_n , \tag{B.4}$$

$$\ddot{\mathbf{u}}_\alpha = \alpha_m\ddot{\mathbf{u}}_{n+1} + (1-\alpha_m)\ddot{\mathbf{u}}_n , \tag{B.5}$$

where the velocity and displacement at time step t_{n+1} are computed by a Newmark update:

$$\mathbf{u}_{n+1} = \mathbf{u}_n + \Delta t \dot{\mathbf{u}}_n + \frac{1}{2}(\Delta t)^2 \left((1-2\beta)\ddot{\mathbf{u}}_n + 2\beta \ddot{\mathbf{u}}_{n+1}\right) , \tag{B.6}$$

$$\dot{\mathbf{u}}_{n+1} = \dot{\mathbf{u}}_n + \Delta t \left((1-\gamma)\ddot{\mathbf{u}}_n + \gamma \ddot{\mathbf{u}}_{n+1}\right) , \tag{B.7}$$

with β and γ as the Newmark parameters and $\Delta t = t_{n+1} - t_n$ as the time step size. Accordingly, the internal and external forces are evaluated as:

$$\mathbf{F}^{int}_{\alpha} = \mathbf{F}^{int}(\mathbf{u}_{\alpha}) , \tag{B.8}$$

$$\mathbf{F}^{ext}_{\alpha} = \mathbf{F}^{ext}(\mathbf{u}_{\alpha}) , \tag{B.9}$$

For displacement-independent loads, $\mathbf{F}^{ext}_{\alpha}$ is simply obtained by:

$$\mathbf{F}^{ext}_{\alpha} = \alpha_f \mathbf{F}^{ext}_{n+1} + (1-\alpha_f)\mathbf{F}^{ext}_{n} . \tag{B.10}$$

The residual (B.1) computed with these interpolated variables is denoted by $\mathbf{R}_{\alpha}$, accordingly. Linearizing and solving (B.1) with respect to the acceleration yields the following equation system:

$$\frac{\mathrm{d}\mathbf{R}_{\alpha}}{\mathrm{d}\ddot{\mathbf{u}}_{n+1}} \Delta \ddot{\mathbf{u}}_{n+1} = -\mathbf{R}_{\alpha} . \tag{B.11}$$

If a linear damping model is considered, i.e., if $\mathbf{C}_d$ is assumed to be constant [72], equation (B.11) becomes:

$$\left(\alpha_m \mathbf{M} + \alpha_f \gamma \Delta t \mathbf{C}_d + \alpha_f \beta (\Delta t)^2 \mathbf{K}(\mathbf{u}_{\alpha})\right) \Delta \ddot{\mathbf{u}}_{n+1} = -\mathbf{M}\ddot{\mathbf{u}}_{\alpha} - \mathbf{C}_d \dot{\mathbf{u}}_{\alpha} - \mathbf{F}^{int}_{\alpha} + \mathbf{F}^{ext}_{\alpha} . \tag{B.12}$$

Alternatively, Eq. (B.1) can be linearized and solved for the displacement:

$$\frac{\mathrm{d}\mathbf{R}_{\alpha}}{\mathrm{d}\mathbf{u}_{n+1}} \Delta \mathbf{u}_{n+1} = -\mathbf{R}_{\alpha} . \tag{B.13}$$

In this case, acceleration and velocity are updated as follows:

$$\ddot{\mathbf{u}}_{n+1} = \frac{1}{\beta(\Delta t)^2}(\mathbf{u}_{n+1} - \mathbf{u}_n) - \frac{1}{\beta \Delta t}\dot{\mathbf{u}}_n - \left(\frac{1}{2\beta} - 1\right)\ddot{\mathbf{u}}_n , \tag{B.14}$$

$$\dot{\mathbf{u}}_{n+1} = \frac{\gamma}{\beta \Delta t}(\mathbf{u}_{n+1} - \mathbf{u}_n) + \left(1 - \frac{\gamma}{\beta}\right)\dot{\mathbf{u}}_n + \left(1 - \frac{\gamma}{2\beta}\right)\Delta t \ddot{\mathbf{u}}_n , \tag{B.15}$$

Considering again a constant $\mathbf{C}_d$, equation (B.13) becomes:

$$\left(\alpha_m \frac{1}{\beta(\Delta t)^2}\mathbf{M} + \alpha_f \frac{\gamma}{\beta \Delta t}\mathbf{C}_d + \alpha_f \mathbf{K}(\mathbf{u}_\alpha)\right)\Delta \mathbf{u}_{n+1} = -\mathbf{M}\ddot{\mathbf{u}}_\alpha - \mathbf{C}_d\dot{\mathbf{u}}_\alpha - \mathbf{F}_\alpha^{int} + \mathbf{F}_\alpha^{ext} \,. \tag{B.16}$$

According to [24, 54], the α and Newmark parameters are determined by the numerical dissipation parameter $\rho_\infty \in [0, 1]$ as follows:

$$\alpha_m = \frac{2 - \rho_\infty}{1 + \rho_\infty} \,, \quad \alpha_f = \frac{1}{1 + \rho_\infty} \,, \quad \beta = \frac{(1 - \alpha_f + \alpha_m)^2}{4} \,, \quad \gamma = \frac{1}{2} - \alpha_f + \alpha_m \,, \tag{B.17}$$

where $\rho_\infty = 0.5$ is adopted in this paper.

Appendix C. Linearization of strain variables

As mentioned in Section 6, we compute the partial derivatives with respect to discrete nodal displacements u_r, which is denoted by $(\cdot)_{,r}$ for a compact notation in the following. We obtain the variation of the displacement vector by (72):

$$\mathbf{u}_{,r} = \frac{\partial \mathbf{u}}{\partial u_r} = N^a \mathbf{e}_i \,,$$

where r is the global degree of freedom number corresponding to the i-th displacement component ($i = 1, 2, 3$ referring x, y, z) of control point a, N^a is the corresponding shape function, and $\mathbf{e}_i$ the global Cartesian base vector. For the second derivatives we obtain:

$$\mathbf{u}_{,rs} = \frac{\partial^2 \mathbf{u}}{\partial u_r \partial u_s} = \mathbf{0} \,. \tag{C.1}$$

Since variations with respect to u_r vanish for all quantities of the undeformed configuration, $(\mathring{\cdot})_{,r} = \mathbf{0}$, we obtain for the variation of the position vector $\mathbf{r} = \mathring{\mathbf{r}} + \mathbf{u}$:

$$\mathbf{r}_{,r} = \mathbf{u}_{,r} = N^a \mathbf{e}_i \,, \tag{C.2}$$

$$\mathbf{r}_{,rs} = \mathbf{u}_{,rs} = \mathbf{0} \,. \tag{C.3}$$

Accordingly, we get the variations of the base vectors $\mathbf{a}_\alpha$ as:

$$\mathbf{a}_{\alpha,r} = N^a_{,\alpha} \, \mathbf{e}_i \,, \tag{C.4}$$

$$\mathbf{a}_{\alpha,rs} = \mathbf{0} \,, \tag{C.5}$$

and for $\mathbf{a}_{\alpha,\beta}$:

$$\mathbf{a}_{\alpha,\beta,r} = N^{,a}_{,\alpha\beta}\,\mathbf{e}_i\ , \tag{C.6}$$

$$\mathbf{a}_{\alpha,\beta,rs} = \mathbf{0}\ . \tag{C.7}$$

With (C.4)–(C.5) and $u_s = u^b_j$, $s = 3(b-1)+j$, we can express the variations of the metric coefficients $a_{\alpha\beta} = \mathbf{a}_\alpha \cdot \mathbf{a}_\beta$ as:

$$a_{\alpha\beta,r} = N^{,a}_{,\alpha}\,\mathbf{e}_i \cdot \mathbf{a}_\beta + N^{,a}_{,\beta}\,\mathbf{e}_i \cdot \mathbf{a}_\alpha\ , \tag{C.8}$$

$$a_{\alpha\beta,rs} = (N^{,a}_{,\alpha}\,N^{,b}_{,\beta} + N^{,a}_{,\beta}\,N^{,b}_{,\alpha})\delta_{ij}\ . \tag{C.9}$$

The variations of the unit normal vector $\mathbf{a}_3$ are more involved and, therefore, we introduce the auxiliary variables $\tilde{\mathbf{a}}_3$ and $\bar{a}_3$:

$$\tilde{\mathbf{a}}_3 = \mathbf{a}_1 \times \mathbf{a}_2\ , \tag{C.10}$$

$$\bar{a}_3 = \sqrt{\tilde{\mathbf{a}}_3 \cdot \tilde{\mathbf{a}}_3}\ , \tag{C.11}$$

such that $\mathbf{a}_3$ can be written as:

$$\mathbf{a}_3 = \frac{\tilde{\mathbf{a}}_3}{\bar{a}_3}\ . \tag{C.12}$$

In the following, we first compute the variations of the auxiliary variables which are then used for further derivations. It is convenient to follow this approach also in the implementation since these intermediate results are needed several times. We first derive the variations of $\tilde{\mathbf{a}}_3$ using also (C.5):

$$\tilde{\mathbf{a}}_{3,r} = \mathbf{a}_{1,r} \times \mathbf{a}_2 + \mathbf{a}_1 \times \mathbf{a}_{2,r}\ , \tag{C.13}$$

$$\tilde{\mathbf{a}}_{3,rs} = \mathbf{a}_{1,r} \times \mathbf{a}_{2,s} + \mathbf{a}_{1,s} \times \mathbf{a}_{2,r}\ , \tag{C.14}$$

which are used for the variations of $\bar{a}_3$:

$$\bar{a}_{3,r} = \mathbf{a}_3 \cdot \tilde{\mathbf{a}}_{3,r}\ , \tag{C.15}$$

$$\bar{a}_{3,rs} = \bar{a}_3^{-1}\,(\tilde{\mathbf{a}}_{3,rs} \cdot \tilde{\mathbf{a}}_3 + \tilde{\mathbf{a}}_{3,r} \cdot \tilde{\mathbf{a}}_{3,s} - (\tilde{\mathbf{a}}_{3,r} \cdot \mathbf{a}_3)(\tilde{\mathbf{a}}_{3,s} \cdot \mathbf{a}_3))\ , \tag{C.16}$$

and finally for the variations of $\mathbf{a}_3$:

$$\mathbf{a}_{3,r} = \bar{a}_3^{-1}(\tilde{\mathbf{a}}_{3,r} - \bar{a}_{3,r}\,\mathbf{a}_3)\ , \tag{C.17}$$

$$\mathbf{a}_{3,rs} = \bar{a}_3^{-1}(\tilde{\mathbf{a}}_{3,rs} - \bar{a}_{3,rs}\,\mathbf{a}_3) + \bar{a}_3^{-2}(2\,\bar{a}_{3,r}\,\bar{a}_{3,s}\,\mathbf{a}_3 - \bar{a}_{3,r}\,\tilde{\mathbf{a}}_{3,s} - \bar{a}_{3,s}\,\tilde{\mathbf{a}}_{3,r})\ . \tag{C.18}$$

The detailed steps of these derivations can be found in [57]. With (C.6)–(C.7) and (C.17)–(C.18), we can compute the variations of the curvatures $b_{\alpha\beta} = \mathbf{a}_{\alpha,\beta} \cdot \mathbf{a}_3$:

$$b_{\alpha\beta,r} = \mathbf{a}_{\alpha,\beta,r} \cdot \mathbf{a}_3 + \mathbf{a}_{\alpha,\beta} \cdot \mathbf{a}_{3,r} \ , \tag{C.19}$$

$$b_{\alpha\beta,rs} = \mathbf{a}_{\alpha,\beta,r} \cdot \mathbf{a}_{3,s} + \mathbf{a}_{\alpha,\beta,s} \cdot \mathbf{a}_{3,r} + \mathbf{a}_{\alpha,\beta} \cdot \mathbf{a}_{3,rs} \ . \tag{C.20}$$

With Eqs. (C.6)–(C.7) and (C.19)–(C.20) we finally obtain the variations of the strain variables:

$$\varepsilon_{\alpha\beta,r} = \frac{1}{2}(a_{\alpha\beta} - A_{\alpha\beta})_{,r} = \frac{1}{2} a_{\alpha\beta,r} \ , \tag{C.21}$$

$$\varepsilon_{\alpha\beta,rs} = \frac{1}{2} a_{\alpha\beta,rs} \ , \tag{C.22}$$

$$\kappa_{\alpha\beta,r} = (B_{\alpha\beta} - b_{\alpha\beta})_{,r} = -b_{\alpha\beta,r} \ , \tag{C.23}$$

$$\kappa_{\alpha\beta,rs} = -b_{\alpha\beta,rs} \ . \tag{C.24}$$

References

[1] M. Bischoff, W.A. Wall, K.-U. Bletzinger, and E. Ramm. Models and finite elements for thin-walled structures. In *Encyclopedia of Computational Mechanics*, volume 2, Solids, Structures and Coupled Problems. Wiley, 2004.

[2] E.N. Dvorkin and K.-J. Bathe. A continuum mechanics based four-node shell element for general non-linear analysis. *Engineering Computations*, 1:77–88, 1984.

[3] B. Brank, J. Korelc, and A. Ibrahimbegovic. Nonlinear shell problem formulation accounting for through-the-thickness stretching and its finite element implementation. *Computers & Structures*, 80:699–717, 2002.

[4] N. Büchter, E. Ramm, and D. Roehl. Three-dimensional extension of non-linear shell formulation based on the enhanced assumed strain concept. *International Journal for Numerical Methods in Engineering*, 37:2551–2567, 1994.

[5] M. Bischoff and E. Ramm. Shear deformable shell elements for large strains and rotations. *International Journal for Numerical Methods in Engineering*, 40(23):4427–4449, 1997.

[6] J.C. Simo, M.S. Rifai, and D.D. Fox. On a stress resultant geometrically exact shell model. part iv: Variable thickness shells with through-the-thickness stretching. *Computer Methods in Applied Mechanics and Engineering*, 81(1):91–126, 1990.

[7] R.A.F. Valente, R.J Alves de Sousa, and R.M. Natal Jorge. An enhanced strain 3D element for large deformation elastoplastic thin-shell applications. *Computational Mechanics*, 34:38–52, 2004.

[8] S. Reese, P. Wriggers, and B.D. Reddy. A new locking-free brick element technique for large deformation problems in elasticity. *Computers & Structures*, 75:291–304, 2000.

[9] M. Schwarze and S. Reese. A reduced integration solid-shell finite element based on the EAS and the ANS concept - Large deformation problems. *International Journal for Numerical Methods in Engineering*, 85:289–329, 2011.

[10] Y. Başar and Y. Ding. Finite-element analysis of hyperelastic thin shells with large strains. *Computational Mechanics*, 18:200–214, 1996.

[11] B. Schieck, W. Pietraszkiewicz, and H. Stumpf. Theory and numerical analysis of shells undergoing large elastic strains. *International Journal for Solids and Structures*, 29(6):689–709, 1991.

[12] E. Oñate and F. Zárate. Rotation-free triangular plate and shell elements. *International Journal for Numerical Methods in Engineering*, 47:557–603, 2000.

[13] J. Linhard, R. Wüchner, and K.-U. Bletzinger. "Upgrading" membranes to shells – The CEG rotation free shell element and its application in structural analysis. *Finite Elements in Analysis and Design*, 44:63–74, 2007.

[14] V. Ivannikov, C. Tiago, and P.M. Pimenta. Meshless implementation of the geometrically exact Kirchhoff–Love shell theory. *International Journal for Numerical Methods in Engineering*, 100(1):1–39, 2014.

[15] F. Cirak, M. Ortiz, and P. Schröder. Subdivision surfaces: a new paradigm for thin shell analysis. *International Journal for Numerical Methods in Engineering*, 47:2039–2072, 2000.

[16] F. Cirak and M. Ortiz. Fully C1-conforming subdivision elements for finite deformation thin-shell analysis. *International Journal for Numerical Methods in Engineering*, 51:813–833, 2001.

[17] T.J.R. Hughes, J.A. Cottrell, and Y. Bazilevs. Isogeometric analysis: CAD, finite elements, NURBS, exact geometry, and mesh refinement. *Computer Methods in Applied Mechanics and Engineering*, 194:4135–4195, 2005.

[18] T.W. Sederberg, J. Zheng, A. Bakenov, and A. Nasri. T-splines and T-NURCCS. *ACM Transactions on Graphics*, 22(3):477–484, 2003.

[19] T. W. Sederberg, D.L. Cardon, G.T. Finnigan, N.S. North, J. Zheng, and T. Lyche. T-spline simplification and local refinement. *ACM Transactions on Graphics*, 23(3):276–283, 2004.

[20] Y. Bazilevs, V.M. Calo, J.A. Cottrell, J.A. Evans, T.J.R. Hughes, S. Lipton, M.A. Scott, and T.W. Sederberg. Isogeometric analysis using T-splines. *Computer Methods in Applied Mechanics and Engineering*, 199:229–263, 2010.

[21] M. Dörfel, B. Jüttler, and B. Simeon. Adaptive Isogeometric Analysis by Local h-Refinement with T-splines. *Computer Methods in Applied Mechanics and Engineering*, 199:264–275, 2010.

[22] Y. Bazilevs, M.-C. Hsu, and M. A. Scott. Isogeometric fluid–structure interaction analysis with emphasis on non-matching discretizations, and with application to wind turbines. *Computer Methods in Applied Mechanics and Engineering*, 249–252:28–41, 2012.

[23] D. Schillinger, L. Dedè, M.A. Scott, J.A. Evans, M.J. Borden, E. Rank, and T.J.R. Hughes. An isogeometric design-through-analysis methodology based on adaptive hierarchical refinement of NURBS, immersed boundary methods, and T-spline CAD surfaces. *Computer Methods in Applied Mechanics and Engineering*, 249–252:116–150, 2012.

[24] J.A. Cottrell, T.J.R. Hughes, and Y. Bazilevs. *Isogeometric Analysis: Toward Integration of CAD and FEA*. Wiley, 2009.

[25] J.A. Cottrell, A. Reali, Y. Bazilevs, and T.J.R. Hughes. Isogeometric analysis of structural vibrations. *Computer Methods in Applied Mechanics and Engineering*, 195:5257–5296, 2006.

[26] J.A. Cottrell, T.J.R. Hughes, and A. Reali. Studies of refinement and continuity in isogeometric structural analysis. *Computer Methods in Applied Mechanics and Engineering*, 196:4160–4183, 2007.

[27] J. Kiendl, K.-U. Bletzinger, J. Linhard, and R. Wüchner. Isogeometric shell analysis with Kirchhoff-Love elements. *Computer Methods in Applied Mechanics and Engineering*, 198:3902–3914, 2009.

[28] N. Nguyen-Thanh, J. Kiendl, H. Nguyen-Xuan, R. Wüchner, K. U. Bletzinger, Y. Bazilevs, and T. Rabczuk. Rotation free isogeometric thin shell analysis using PHT-splines. *Computer Methods in Applied Mechanics and Engineering*, 200(47-48):3410–3424, 2011.

[29] D. J. Benson, Y. Bazilevs, M.-C. Hsu, and T. J. R. Hughes. A large deformation, rotation-free, isogeometric shell. *Computer Methods in Applied Mechanics and Engineering*, 200:1367 – 1378, 2011.

[30] T.-K. Uhm and S.-K. Youn. T-spline finite element method for the analysis of shell structures. *International Journal for Numerical Methods in Engineering*, 80:507–536, 2009.

[31] D. J. Benson, Y. Bazilevs, M. C. Hsu, and T. J. R. Hughes. Isogeometric shell analysis: The Reissner-Mindlin shell. *Computer Methods in Applied Mechanics and Engineering*, 199:276 – 289, 2010.

[32] W. Dornisch, S. Klinkel, and B. Simeon. Isogeometric Reissner-Mindlin shell analysis with exactly calculated director vectors. *Computer Methods in Applied Mechanics and Engineering*, 253:491–504, 2013.

[33] W. Dornisch and S. Klinkel. Treatment of Reissner-Mindlin shells with kinks without the need for drilling rotation stabilization in an isogeometric framework. *Computer Methods in Applied Mechanics and Engineering*, 276:35–66, 2014.

[34] D.J. Benson, S. Hartmann, Y. Bazilevs, M.-C. Hsu, and T.J.R. Hughes. Blended isogeometric shells. *Computer Methods in Applied Mechanics and Engineering*, 255:133–146, 2013.

[35] R. Echter, B. Oesterle, and M. Bischoff. A hierarchic family of isogeometric shell finite elements. *Computer Methods in Applied Mechanics and Engineering*, 254(0):170 – 180, 2013.

[36] S. Hosseini, J.J.C. Remmers, C.V. Verhoosel, and R. de Borst. An isogeometric solid-like shell element for nonlinear analysis. *International Journal for Numerical Methods in Engineering*, 95:238–256, 2013.

[37] S. Hosseini, J.J.C. Remmers, C.V. Verhoosel, and R. de Borst. An isogeometric continuum shell element for non-linear analysis. *Computer Methods in Applied Mechanics and Engineering*, 271:1–22, 2014.

[38] R. Bouclier, T. Elguedj, and A. Combescure. Efficient isogeometric NURBS-based solid-shell elements: Mixed formulation and B-bar-method. *Computer Methods in Applied Mechanics and Engineering*, 267:86–110, December 2013.

[39] J.F. Caseiro, R.A.F. Valente, A. Reali, J. Kiendl, F. Auricchio, and R.J Alves de Sousa. On the Assumed Natural Strain method to alleviate locking in solid-shell NURBS-based finite elements. *Computational Mechanics*, 53:1341–1353, 2014.

[40] J.F. Caseiro, R.A.F. Valente, A. Reali, J. Kiendl, F. Auricchio, and R.J Alves de Sousa. Assumed Natural Strain NURBS-based solid-shell element for the analysis of large deformation

elasto-plastic thin-shell structures. *Computer Methods in Applied Mechanics and Engineering*, 284:861–880, 2015.

[41] R. Schmidt, J. Kiendl, K.-U. Bletzinger, and R. Wüchner. Realization of an integrated structural design process: analysis–suitable geometric modelling and isogeometric analysis. *Computing and Visualization in Science*, 13(7):315–330, 2010.

[42] M. Breitenberger, A. Apostolatos, B. Philipp, R. Wüchner, and K.-U. Bletzinger. Analysis in computer aided design: Nonlinear isogeometric B-Rep analysis of shell structures. *Computer Methods in Applied Mechanics and Engineering*, 284:401–457, 2015.

[43] Y. Bazilevs, M.-C. Hsu, J. Kiendl, R. Wüchner, and K.-U. Bletzinger. 3D simulation of wind turbine rotors at full scale. Part II: Fluid-structure interaction modeling with composite blades. *International Journal for Numerical Methods in Fluids*, 65(1-3):236–253, 2011.

[44] M.-C. Hsu and Y. Bazilevs. Fluid–structure interaction modeling of wind turbines: simulating the full machine. *Computational Mechanics*, 50:821–833, 2012.

[45] Y. Bazilevs, M.-C. Hsu, J. Kiendl, and D. J. Benson. A computational procedure for prebending of wind turbine blades. *International Journal for Numerical Methods in Engineering*, 89:323–336, 2012.

[46] A. Korobenko, M.-C. Hsu, I. Akkerman, J. Tippmann, and Y. Bazilevs. Structural mechanics modeling and FSI simulation of wind turbines. *Mathematical Models and Methods in Applied Sciences*, 23(02):249–272, 2013.

[47] J. Lu and C. Zheng. Dynamic cloth simulation by isogeometric analysis. *Computer Methods in Applied Mechanics and Engineering*, 268:475–493, 2014.

[48] L. Chen, N. Nguyen-Thanh, H. Nguyen-Xuan, T. Rabczuk, S.P.A. Bordas, and G. Limbert. Explicit finite deformation analysis of isogeometric membranes. *Computer Methods in Applied Mechanics and Engineering*, 277(104-130), 2014.

[49] N. Nguyen-Thanh, N. Valizadeh, M.N. Nguyen, H. Nguyen-Xuan, X. Zhuang, P. Areias, G. Zi, Y. Bazilevs, L. De Lorenzis, and T. Rabczuk. An extended isogeometric thin shell analysis based on Kirchhoff–Love theory. *Computer Methods in Applied Mechanics and Engineering*, 284:265–291, 2015.

[50] G. A. Holzapfel. *Nonlinear Solid Mechanics, a Continuum Approach for Engineering*. Wiley, Chichester, 2000.

[51] Y. Bazilevs, M.-C. Hsu, D.J. Benson, S. Sankaran, and A.L. Marsden. Computational fluid–structure interaction: methods and application to a total cavopulmonary connection. *Computational Mechanics*, 45:77–89, 2009.

[52] S. Klinkel and S. Govindjee. Using finite strain 3D-material models in beam and shell elements. *Engineering Computations*, 19(8):902–921, 2002.

[53] J.C. Simo and C. Miehe. Associated coupled thermoplasticity at finite strains: formulation, numerical analysis and implementation. *Computer Methods in Applied Mechanics and Engineering*, 98(1):41–104, 1992.

[54] J. Chung and G. M. Hulbert. A time integration algorithm for structural dynamics with improved numerical dissipation: The generalized-α method method. *Journal of Applied Mechanics*, 60:371–75, 1993.

[55] L. Piegl and W. Tiller. *The NURBS Book*. Springer-Verlag, New York, 2nd edition, 1997.

[56] D.F. Rogers. *An Introduction to NURBS With Historical Perspective*. Academic Press, San Diego, CA, 2001.

[57] J. Kiendl. *Isogeometric Analysis and Shape Optimal Design of Shell Structures*. PhD thesis, Technische Universtität München, 2011.

[58] M.A. Scott, M.J. Borden, C.V. Verhoosel, T.W. Sederberg, and T.J.R. Hughes. Isogeometric finite element data structures based on Bézier extraction of T-splines. *International Journal for Numerical Methods in Engineering*, 88:126–156, 2011.

[59] J. Kiendl, Y. Bazilevs, M.-C. Hsu, R. Wüchner, and K.-U. Bletzinger. The bending strip method for isogeometric analysis of Kirchhoff-Love shell structures comprised of multiple patches. *Computer Methods in Applied Mechanics and Engineering*, 199:2403–2416, 2010.

[60] A. Apostolatos, R. Schmidt, R. Wüchner, and K.-U. Bletzinger. A Nitsche-type formulation and comparison of the most common domain decomposition methods in isogeometric analysis. *International Journal for Numerical Methods in Engineering*, 97:473–504, 2013.

[61] Y. Guo and M. Ruess. Nitsche's method for a coupling of isogeometric thin shells and blended shell structures. *Computer Methods in Applied Mechanics and Engineering*, 284:881–905, 2015.

[62] Y. C. Fung. *Biomechanics: Mechanical Properties of Living Tissues*. Springer-Verlag, New York, second edition, 1993.

[63] W. Sun, M. S. Sacks, T. L. Sellaro, W. S. Slaughter, and M. J. Scott. Biaxial mechanical response of bioprosthetic heart valve biomaterials to high in-plane shear. *Journal of Biomechanical Engineering*, 125(3):372–380, 2003.

[64] C.-H. Lee, R. Amini, R. C. Gorman, J. H. Gorman, and M. S. Sacks. An inverse modeling approach for stress estimation in mitral valve anterior leaflet valvuloplasty for in-vivo valvular biomaterial assessment. *Journal of Biomechanics*, 47(9):2055–2063, 2014.

[65] W. Sun, A. Abad, and M. S. Sacks. Simulated bioprosthetic heart valve deformation under quasi-static loading. *Journal of Biomechanical Engineering*, 127(6):905–914, 2005.

[66] H. Kim, J. Lu, M. S. Sacks, and K. B. Chandran. Dynamic simulation of bioprosthetic heart valves using a stress resultant shell model. *Annals of Biomedical Engineering*, 36(2):262–275, 2008.

[67] D. Kamensky, M.-C. Hsu, D. Schillinger, J. A. Evans, A. Aggarwal, Y. Bazilevs, M. S. Sacks, and T. J. R. Hughes. An immersogeometric variational framework for fluid–structure interaction: Application to bioprosthetic heart valves. *Computer Methods in Applied Mechanics and Engineering*, 284:1005–1053, 2015.

[68] M.-C. Hsu, D. Kamensky, Y. Bazilevs, M. S. Sacks, and T. J. R. Hughes. Fluid–structure interaction analysis of bioprosthetic heart valves: significance of arterial wall deformation. *Computational Mechanics*, 54(4):1055–1071, 2014.

[69] M. A. Scott, X. Li, T. W. Sederberg, and T. J. R. Hughes. Local refinement of analysis-suitable T-splines. *Computer Methods in Applied Mechanics and Engineering*, 213-216:206–222, 2012.

[70] Autodesk T-Splines Plug-in for Rhino. http://www.tsplines.com/products/tsplines-for-rhino.html. 2014.

[71] M. A. Scott, T. J. R. Hughes, T. W. Sederberg, and M. T. Sederberg. An integrated approach to engineering design and analysis using the Autodesk T-spline plugin for Rhino3d. ICES REPORT 14-33, The Institute for Computational Engineering and Sciences, The University of Texas at Austin, September 2014, 2014.

[72] P. Wriggers. *Nonlinear Finite Element Methods*. Springer, 2008.